

書籍購入の仕組みの説明

医学書販売店

このサイトについて

会社案内

個人情報保護ポリシー

特定商取引法に基づく表示

正誤表

本郷昔語り

リンク集

全血製剤

- 1 抗凝固液, 保存液 / 11
- 2 保存容器 / 13
- 3 保存温度 / 13
- 4 放射線照射 / 13
- 5 使用適応, 供給 / 14
- 6 感染症検査 / 14

赤血球製剤

- 1 種類 / 15
- 2 製造, 保存容器 / 16
- 3 保存温度, 保存・使用期間 / 17
- 4 保存中の生化学的性状変化 / 18
- 5 使用適応 / 20
- 6 使用量, 期待Hb上昇値 / 22

血小板製剤

- 1 種類 / 23
- 2 製造, 保存 / 25
- 3 保存による変化 / 26
- 4 使用適応 / 28
- 5 投与後予測増加量 / 29
- 6 ABO 型適合血小板輸血 / 30
- 7 血小板輸血セット / 30

新鮮凍結血漿 (fresh frozen plasma : FFP)

- 1 製造, 保存, 供給 / 31
- 2 使用法 / 32
- 3 適応 / 33
- 4 使用注意事項 / 35

アルブミン製剤

- 1 製造, 製品 / 36
- 2 アルブミンの特性 / 36
- 3 使用適応 / 37
- 4 投与量, 投与法 / 39
- 5 注意事項 / 39

その他の血液製剤

- 1 アンチトロンビン[◆] (antithrombin[◆] : AT[◆]) / 40
- 2 ハプトグロビン / 40
- 3 グロブリン製剤, 凝固因子製剤 / 41

冷凍血液

- 1 凍結赤血球 / 41
- 2 凍結血小板 / 44
- 3 凍結血漿, 新鮮凍結血漿 (FFP) / 45

III. 血液型

赤血球の抗原, 抗体

- 1 ABO型 / 51
- 2 Rh 型 / 54
- 3 その他の血液型 / 56

- 4 不規則抗体／60
- 5 交差適合試験／62
- 白血球抗原（リンパ球抗原：human lymphocyte antigen：HLA）
- 血小板抗原
 - 血小板上の抗原性の臨床的意義／64
- 血清蛋白抗原

IV. 輸血療法の実際

予定手術での輸血

- 1 輸血既往歴、妊娠歴の確認／71
- 2 生理機能検査／71
- 3 赤血球製剤準備量／71
- 4 交差試験／74
- 5 手術前輸血／74
- 6 輸血施行手順／75

緊急時の輸血

- 1 循環血液量の維持、末梢循環改善／79
- 2 血液型判定とO型血液使用／80
- 3 制御しがたい出血（uncontrollable hemorrhage）／80

大量輸血、急速輸血

- 1 血液Hb量の維持／83
- 2 赤血球製剤投与と循環血液量の調整／83
- 3 急速輸血実施法／84
- 4 赤血球製剤の大量・急速輸血時の注意／84
- 5 使用する赤血球製剤の血液型の検査確認／84
- 6 FFP、血小板の使用／85
- 7 自己血の利用／86

新生児・小児での輸血

- 1 赤血球輸血／86
- 2 血小板輸血／89
- 3 FFP輸血／89
- 4 インフォームドコンセントの取得／89
- 5 サイトメガロウイルス感染／90

高齢者、心疾患患者への輸血

輸血路の確保

輸血必要機器・材料

- 1 留置針、留置カニューレ、静脈カテーテル／92
- 2 輸血セット／92
- 3 特殊輸血フィルタ／93
- 4 急速輸血器／94
- 5 血液加温装置／94

患者監視

- 1 全身状態、バイタルサイン（vital signs）／95
- 2 循環血液量、中心静脈圧／95
- 3 血液凝固・止血機能／96
- 4 心電図／96

- 5 体温／96
- 自己血輸血
- 白血球（顆粒球）輸血

V. 輸血事故，輸血副作用・合併症

- 輸血事故
 - 1 技術的な過誤（technical error）／105
 - 2 事務管理上の過誤（clerical error）／106
- 輸血副作用・合併症
 - 1 免疫的合併症／108
 - 2 輸血感染症／123
 - 3 輸血手技関連合併症／131
 - 4 血液製剤の作製，製造，保存に伴う合併症／135
 - 5 そのほかの合併症／151

VI. 自己血輸血

- 自己血輸血の意義，必要性
 - 1 患者本人への利益／167
 - 2 国家・社会的貢献／169
 - 3 自己血輸血の問題点／170
- 自己血輸血の種類
- 貯血式自己血輸血
 - 1 適応症例／172
 - 2 採血，保存管理／172
 - 3 輸血時の注意／173
 - 4 エリスロポエチンの使用／173
- 希釈式自己血輸血
 - 1 適応症例／174
 - 2 採血，保存，輸血／175
 - 3 希釈式自己血輸血の利点と欠点／175
 - 4 hypervolemic hemodilution（血液量増量自己血輸血）／176
- 回収式自己血輸血
 - 1 種類，名称／176
 - 2 原理，操作／177
 - 3 適応，禁忌／178
- その他の自己血液成分の輸血
 - 1 自己血小板／179
 - 2 自己血漿／180
 - 3 自己クリオプレシピレート（自己フィブリン糊）／180

VII. 人工血液

- 人工赤血球代替物（人工酸素運搬体）
 - 1 ヘモグロビン型酸素運搬体（Hb based oxygen carrier）／188

- 2 PFC 型人工酸素運搬体 (PFC based oxygen carrier) / 193
 - 3 リポソームヘム (liposomeheme) / 196
 - 4 アルブミンヘム (albumin heme) / 199
 - 5 人工酸素運搬体の臨床応用 / 201
- 人工血小板

VIII. 輸血医療に関連した法的規則事項

特定生物由来製品の使用

- 1 患者への説明と同意 (informed consent : IC) / 212
- 2 使用記録保管義務 / 215
- 3 感染症情報の提供、遡及調査の義務付け / 215
- 4 血液製剤の適正使用 / 215

宗教上の理由による輸血拒否

- 1 患者の輸血拒否の確認、医療者側の対策検討 / 216
- 2 患者への説明 / 216

小児への輸血

緊急輸血に伴うO 型血液使用、放射線非照射血液使用

院内採血に伴う検査の限界

医師の守秘保持義務と個人情報保護法

輸血医療に関連する法規

IX. 輸血に関連する歴史的事項

文献的確認が十分に得られない時代の事項

文献的確認が得られている歴史的事項

[その他のシリーズはこちら->](#)

[このページのtopに戻る](#)

[| ホーム |](#) [書籍購入の方法 |](#) [会社案内 |](#) [本郷昔語り |](#) [サイトマップ |](#) [お問い合わせ |](#)

Copyright(C)2006 KOKUSEIDO CO. LTD ALL Rights Reserved

Selective uptake of surface-modified phospholipid vesicles by bone marrow macrophages *in vivo*

Keitaro Sou^a, Beth Goins^b, Shinji Takeoka^a, Eishun Tsuchida^{a,*}, William T. Phillips^b

^aAdvanced Research Institute for Science and Engineering, Waseda University, Tokyo 169-8555, Japan

^bDepartment of Radiology, University of Texas Health Science Center at San Antonio, 7703 Floyd Curl Drive, San Antonio, TX 78229-3900, USA

Received 29 August 2006; accepted 31 January 2007

Available online 20 February 2007

Abstract

An advantage of using vesicles (liposomes) as drug delivery carriers is that their pharmacokinetics can be controlled by surface characteristics, which can permit specific delivery of the encapsulated agents to organs or cells *in vivo*. Here we report a vesicle formulation which targets the bone marrow after intravenous injection in rabbits. Surface modification of the vesicle with an anionic amphiphile; L-glutamic acid, N-(3-carboxy-1-oxopropyl)-, 1,5-dihexadecyl ester (SA) results in significant targeting of vesicles to bone marrow. Further incorporation of as little as 0.6 mol% of poly(ethylene glycol)-lipid (PEG-DSPE) passively enhanced the distribution of SA-vesicles into bone marrow and inhibited hepatic uptake. In this model, more than 60% of the intravenously injected vesicles were distributed to bone marrow within 6 h after administration of a small dose of lipid (15 mg/kg b.w.). Histological evidence indicates that the targeting was achieved due to uptake by bone marrow macrophages (BMM ϕ). The efficient delivery of encapsulated scintigraphic and fluorescent imaging agents to BMM ϕ suggests that vesicles are promising carriers for the specific targeting of BMM ϕ and may be useful for delivering a wide range of therapeutic agents to bone marrow.

© 2007 Elsevier Ltd. All rights reserved.

Keywords: Nanoparticle; Liposome; Bone marrow; Macrophage; Drug delivery; Surface modification

1. Introduction

Nanoparticulate carrier systems have been investigated as candidates for targeted delivery in cancer therapy and gene therapy [1,2]. A wide variety of nanoparticle systems have been developed for biological applications. One of the advantages of using nanoparticulate materials is based on their controllable surface properties which permit specific interactions with cells, tissues, and organs. Although a number of investigators have demonstrated that endocytosis of nanoparticles *in vitro* is accelerated by surface modification of the particles with specific ligands, the specific *in vivo* targeting of cells remains challenging because it is hindered by competing interactions, especially

fairly high mononuclear phagocyte system (MPS) uptake *in vivo*.

Phospholipid vesicles (liposomes) have been widely investigated as potential carriers for drugs, genes, and proteins because their capsular structure permits encapsulation of various therapeutic agents [2–4]. Because of their particulate nature, these vesicles are trapped in the MPS, particularly hepatic Kupffer cells and spleen macrophages following intravenous administration [5,6]. Once in the bloodstream, the binding of plasma proteins such as immunoglobulins, complement proteins, apolipoproteins, etc., which together are termed “opsonins” on the vesicular surface have been reported to accelerate phagocytosis of the vesicles by macrophages, because the macrophages have scavenger receptors to bind the opsonins [5]. In addition to this mechanism, vesicles containing anionic phospholipids such as phosphatidylserine (PS), which are markers of apoptotic cells, have been reported to bind with a PS receptor on macrophages [7]. Improved vesicles with

*Corresponding author. Tel.: +81 3 5286 3120; fax: +81 3 3205 4740.

E-mail addresses: ksou@waseda.jp (K. Sou), eishun@waseda.jp (E. Tsuchida).

prolonged circulation times preventing MPS uptake have been formulated with poly(ethylene glycol) (PEG) derivatives [8]. These vesicles have been termed as stealth liposomes, due to their ability to evade uptake by the macrophage, particularly Kupffer cells. Long circulating liposomes with PEG surface modification are currently being used as anti-cancer drug delivery agents [9].

On the other hand, the phagocytic ability of the MPS contributes to achieving an active targeting of particulate carriers to macrophages [10,11]. Macrophages produce a wide range of biologically active molecules that are both beneficial and detrimental. Many of the detrimental effects of macrophages are associated with their pro-inflammatory effects. Thus, interventions targeted to macrophages may open new therapeutic approaches for controlling diseases associated with inflammation. Evidence from a number of sources suggests that cancer-associated inflammation promotes tumor growth and progression, and tumor-associated macrophages play a critical role in the initiation, maintenance, and resolution of inflammation [12]. These tumor-associated macrophages are inactivated by mediators from tumor cells, and they serve to promote tumor growth. The importance of macrophages in disease development has led a number of researchers to investigate methods for the site-specific delivery of drugs to macrophages.

Bone marrow, which contains macrophages, is one of the organs responsible for uptake of circulating particulate materials [5,9,13–17]. Also, macrophages associated with erythroblasts in a hematopoietic environment participate in erythropoiesis control, and engulfment of nuclei from erythroid precursor cells [18,19]. The development of drug delivery systems with specific bone marrow targeting may have therapeutic benefits for hematological malignancies as well as hemopoiesis control. However, very little attention has been paid to bone marrow as part of the MPS because its contribution to the overall MPS is generally much less than that of the liver and spleen *in vivo*. Another essential problem for targeting of BMM ϕ is caused by lack of understanding of their specific targeting receptor. Therefore, development of a method for specifically targeting bone marrow will be facilitated by knowledge of the strategies to allow nanoparticles to escape from liver and spleen uptake, but not from bone marrow uptake, and development of specific ligands to induce targeting of bone marrow MPS.

Recently, we have discovered a vesicular formulation which shows remarkable targeting to rabbit bone marrow even when administered at small lipid doses. In this article, we address the components of this vesicle responsible for the targeting of bone marrow and additional vesicular modifications for escaping from liver and spleen uptake, but not from bone marrow. These results may be widely applied to the design of nanoparticulate carriers that target the bone marrow. Bone marrow targeting carriers could open up a wide variety of new therapeutic applications.

2. Materials and methods

2.1. Materials

1,2-Dipalmitoyl-*sn*-glycero-3-phosphocholine (DPPC) and cholesterol (CH) were purchased from Nippon Fine Chemical Co. Ltd. (Osaka, Japan); 1,2-distearoyl-*sn*-glycero-3-phosphoethanolamine-*N*-[monomethoxy poly(ethylene glycol) (5000)] (PEG-DSPE) was purchased from NOF Co. (Tokyo, Japan). L-glutamic acid, *N*-(3-carboxy-1-oxopropyl)-, 1,5-dihexadecyl ester (SA) was synthesized as previously reported [20]. Glutathione was purchased from Sigma (St. Louis, MO). Superoxide dismutase (SOD) was purchased from Wako Pure Chemical Industries Ltd. (Osaka, Japan). 4,4-difluoro-5-methyl-4-bora-3a,4a-diaza-s-indacene-3-dodecanoic acid (C₁-BODIPY C₁₂) and Texas Red (TR) sulfonyl chloride were purchased from Molecular Probes, Inc. (Eugene, OR).

2.2. Preparation of vesicles

All vesicle preparations were performed under sterile conditions. DPPC and CH (1:1 molar ratio), or DPPC, CH, and SA (1:1:0.2 molar ratio) were dissolved in benzene and lyophilized to lipid powders. The mixed lipid powder was hydrated with a glutathione (30 mM) and NaCl (120 mM) solution (pH: 7.0) at 5 g dL⁻¹, and submitted to three cycles of freeze-thawing. After controlling vesicle size by an extrusion method (final pore size of the filter: 0.22 μ m, Fuji microfilter, Fuji Photo Film Co., Tokyo, Japan), the unencapsulated glutathione was removed by three ultracentrifugation steps (3 \times 10⁵g, 60 min each) and the vesicles were dispersed in saline solution. Surface modification with PEG was performed by making use of the spontaneous incorporation of PEG-DSPE into vesicles [21]. Various concentrations of the PEG-DSPE dispersion were added to the vesicle dispersion and the mixture incubated at 37°C for 3 h. The vesicle dispersion was ultracentrifuged (3 \times 10⁵g, 60 min) to remove unincorporated PEG-DSPE in the supernatant. After washing the precipitated vesicle pellet by ultracentrifugation (3 \times 10⁵g, 60 min), the PEG-modified vesicles (PEG-vesicles) were dispersed in saline at 7 g dL⁻¹, and the dispersion was then passed through a sterilized membrane filter (pore size 0.45 μ m, DISMIC filter 45, ADVANTEC). The amount of PEG-DSPE incorporated was determined from the peak area ratio of methylene protons of PEG-DSPE (3.63 ppm) to the choline methyl protons of DPPC (3.39 ppm) using ¹H-NMR spectroscopy (JEOL JNM-LA500) [21]. SA-vesicles containing 0.3, 0.6, 1.4, and 2.6 mol% of PEG-DSPE on the surface (represented as PEG(0.3)-, PEG(0.6)-, PEG(1.4)-, and PEG(2.6)-[SA-Ve], respectively) and control vesicles containing 2.6 mol% of PEG-DSPE (represented as PEG(2.6)-Ve) were prepared and characterized for these studies. The diameter of the resulting vesicles was determined with a COULTER submicron particle analyzer (N4SD, Coulter, Hialeah, FL), and represented as an average diameter \pm standard deviation (SD). Endotoxin contamination was determined to be below 0.1 EU/mL by the Limulus assay test [22].

2.3. Technetium-99m (^{99m}Tc)-labeling of vesicles

Radiolabeling of vesicles was performed according to a method described previously [14,17,23,24]. A saline solution of sodium [^{99m}Tc]pertechnetate (5 mL, 2.78 GBq (75 mCi)) (GE Healthcare Radiopharmacy, San Antonio, TX) was injected into a vial containing lyophilized hexamethylpropyleneamine oxime (HMPAO; 0.5 mg, SnCl₂; 7.6 μ g) (CeretekTM; GE Healthcare, Arlington, IL). The mixed solution was incubated for 5 min at room temperature. The ^{99m}Tc-HMPAO solution (1 mL) was then added to the vesicle dispersion ([lipids] = 7 g dL⁻¹, 1 mL), and the resulting mixture was incubated for 1 h. After removing free ^{99m}Tc-HMPAO by gel filtration (Sephadex-G25 column), total radioactivity was measured in a dose calibrator (Radex, Mark 5 Model, Houston, TX) and the labeling efficiency was calculated as the percentage of radioactivity in ^{99m}Tc-vesicles to radioactivity measured just before gel filtration.

2.4. Labeling stability of ^{99m}Tc -labeled vesicles *in vitro*

Labeling stability was examined *in vitro* according to a previously reported procedure [25]. Prepared ^{99m}Tc -labeled vesicle dispersions (0.5 mL) were mixed with rabbit serum (1.5 mL) and incubated at 37 °C to check the labeling stability. A 100 μL aliquot of incubated sample at 24 and 48 h after mixing was passed through a Bio Gel A-15m (200–400 mesh) spin column. The sample was eluted by sequential addition of 100 μL of Dulbecco's phosphate-buffered saline (pH 7.3) under the centrifugal force of 1000 rpm for 1 min. Each fraction was collected separately and counted in a scintillation well counter (Canberra multichannel analyzer; Canberra Industries, Meriden, CT). Another 100 μL aliquot of incubation sample was used as a standard. The sum total of activity eluted with vesicle fractions was compared with total radioactivity in the standard. As for ^{99m}Tc -labeled PEG(0.6)-[SA-Ve], the labeling stability was also examined in human plasma at 37 °C for 24 h.

2.5. Animal experiments

Animal experiments were performed under the National Institutes of Health Animal Use and Care guidelines and approved by the University of Texas Health Science Center at San Antonio Institutional Animal Care Committee. Male New Zealand White rabbits (2–3 kg, $n = 3$ –4 per each vesicle formulation) were anesthetized with an intramuscular injection of ketamine/xylazine (both from Phoenix Scientific, St. Joseph, MO) mixture (50 and 10 mg/kg body weight (b.w.), respectively). One ear of a rabbit was catheterized with a venous line, and the other ear was catheterized with an arterial line. ^{99m}Tc -vesicles were infused into the venous line at 1 mL/min and blood samples were drawn from the arterial line. Each rabbit received a total dose of 214.6–377.4 MBq (5.8–10.2 mCi) ^{99m}Tc -activity and 15 mg/kg b.w. of lipids. As a control study, ^{99m}Tc -HMPAO solution (3 mL) was mixed with glutathione solution (30 mM, 3 mL), and the mixed solution was infused into the venous line at 1 mL/min in rabbits. Each rabbit received a total dose of 321.9–399.6 MBq (8.7–10.8 mCi) ^{99m}Tc -activity.

2.6. Imaging study

Rabbits were placed in the supine position under a Picker (Cleveland, OH) large-field-of-view gamma camera using a low-energy all-purpose collimator and interfaced with a Pinnacle imaging computer (Medasys, Ann Arbor, MI). One-minute dynamic 64×64 pixel scintigraphic images were acquired over a continuous period of 1.5 h after the injection of ^{99m}Tc -vesicles. Static images were also acquired at various times post-injection. The image analysis was performed using a nuclear medicine analysis workstation (Pinnacle computer; Medasys, Ann Arbor, MI). The regions of interest were drawn around images of the whole body, one femur, liver, and spleen. The radioactivity counts were decay-corrected at each time, and converted to a percentage of whole body counts. Corrections were made for the blood pool contribution of each organ using the percent injected dose (%ID) measured immediately after infusion.

2.7. Blood persistence and biodistribution

Blood was collected from the arterial line of the rabbit (100 μL) at various times post-injection. The radioactivity of blood samples was quantified in a scintillation well counter (Canberra Multichannel Analyzer, Meriden, CT) during the same counting session. The counts at each time were converted to the percentage of the counts in the sample collected immediately after injection. The animals were rapidly sacrificed at 6 or 24 h and the tissue samples were collected, weighed and counted for radioactivity in the same scintillation well counter for calculation of biodistribution. To calculate the %ID per organ, total blood volume, muscle and skin mass were estimated as 5.7%, 45%, and 10% of total body weight, respectively [26,27]. Bone mass was estimated to be 12 times that of one femur [28].

2.8. Microscopic study

Histological examination of fluorescence delivered into bone marrow tissues was performed using PEG(0.6)-[SA-Ve], double fluorescently labeled by encapsulating SOD conjugated by TR sulfonyl chloride (TR-SOD) in inner aqueous phase and embedding C₁-BODIPY C₁₂ in bilayer membrane. Conjugation of TR-SOD to SOD was performed according to previously reported procedure [29], and purified TR-SOD was encapsulated in mixed lipids including 1 mol% of C₁-BODIPY C₁₂ to obtain the double fluorescently-labeled PEG(0.6)-[SA-Ve] with size of 247 ± 22 nm in diameter. Labeled vesicles were i.v. injected into anesthetized Male New Zealand White rabbits (2.5 kg, lipids: 15 mg/kg b.w.). At 6 h after injection, femoral bone marrow tissues, liver and spleen were taken, fixed in 10% formalin solution, and then sliced into sections. The sections were fixed on the glass slides with agar at 4 °C and examined with a confocal scanning microscope (Olympus IX-70). Transmission electron microscopic (TEM) observation was performed to observe the bone marrow tissues at a higher magnification. PEG(0.6)-[SA-Ve] were i.v. injected into anesthetized Male New Zealand White rabbits (2.5 kg). The rabbits received 15 mg/kg b.w. of lipids. Control rabbits received no injection. Bone marrow was taken from the left femur of rabbits at 6 h after injection of vesicles, and fixed in 2.5% glutaraldehyde solution. The fixed bone marrow was then washed with 0.1 mol/L phosphate buffer, pH 7.4, and stained with 2% osmic acid solution at 4 °C for 2 h. The organs were first dehydrated stepwise with ethanol, and then polymerized using Quetol 812 at 60 °C for 28 h. The obtained samples were sliced into sections by using an Ultracut S microtome. The sliced samples were stained with 3% uranyl acetate solution for 20 min and then treated with Satoh's lead solution (lead acetate, lead nitrate, and lead citrate) in citrate for 5 min, washed, and dried. The sample was observed and a picture taken with a transmission electron microscope (TEM, H-7500, Hitachi, Tokyo, Japan).

2.9. Theoretical estimation

The theoretical estimation for surface coverage by PEG on vesicles has been reported previously [30,31]. At low grafting densities of PEG, the chains of grafted-PEG are displayed "mushrooms", in which area A_{PEG} covered by each molecule is theoretically calculated as

$$A_{\text{PEG}} = \pi R_F^2, \quad (1)$$

where the Flory radius R_F is given by

$$R_F = N^{3/5} a, \quad (2)$$

where N is the degree of polymerization, a is the size of a monomer.

The percentage of covered surface area by PEG in the mushroom conformation R was estimated as

$$R = A_{\text{PEG}} \times M / A_{\text{lipid}}, \quad (3)$$

where M is the mole percentage of PEG-DSPE and A_{lipid} is the average area of total membrane lipids. In subsequent calculation, we used $N = 114$ and $a = 0.35$ nm for PEG (Mw 5000), and $A_{\text{lipid}} \approx 0.4$ nm² for average area as mixed membrane of DPPC and CH (1:1 molar ratio) [32].

2.10. Statistical methods

Values are reported as mean \pm standard error of the mean (SEM). Statistical analysis was performed using Microsoft Excel for Windows. Biodistribution data were compared using the Student's unpaired *t*-test. A *p*-value < 0.01 or 0.05 was considered statistically significant.

3. Results

3.1. Surface modification and radiolabeling

The average diameter of vesicles was controlled to 270 nm by the stepwise extrusion through cellulose acetate membrane filters with a final pore size of 0.22 μm as shown in Table 1. The surface of the vesicles were modified during spontaneous incorporation of PEG conjugated to 1,2-distearoyl-*sn*-glycero-3-phosphoethanolamine (DSPE) into the lipid bilayer of preformed vesicles. The incorporation efficiency of PEG-DSPE was approximately 85%, independent of the added amount. Theoretically, the surface of PEG (0.3)-[SA-Ve] is not fully covered with PEG chains in mushroom conformation (theoretically calculated covered surface area: 85%), and surface coverage is completed with >0.6 mol% of PEG-DSPE. The $^{99\text{m}}\text{Tc}$ -labeling efficiency was approximately 84%, independent of the vesicular formulation. Since the $^{99\text{m}}\text{Tc}$ was located in the inner aqueous phase of vesicles encapsulating glutathione, the surface properties would not have been altered by the labeling procedure. The incubation of labeled $^{99\text{m}}\text{Tc}$ -vesicles in rabbit serum for 48 h revealed that more than 95% of the incorporated $^{99\text{m}}\text{Tc}$ remained in the prepared vesicles, regardless of the composition of the vesicles. Also in human plasma, 98% of incorporated $^{99\text{m}}\text{Tc}$ remained with PEG(0.6)-[SA-Ve] at 24 h. These data indicate that the labeling procedure results in a stably labeled vesicle preparation and maintains the $^{99\text{m}}\text{Tc}$ within vesicles, even during incubation in plasma at 37 °C.

3.2. Circulation kinetics and biodistribution

First, the circulation kinetics and organ distribution of several formulations were compared to determine the optimized component for targeting bone marrow. For this purpose, scintigraphy was superior to other methods because it was possible to quantitatively determine the organ distribution of the injected vesicles in whole body. The elimination rate of SA-Ve from circulating blood was much faster compared with that of control vesicles (Ve): the circulating half-life times ($t_{1/2\text{s}}$) of the SA-Ve and Ve

were 0.6 and 9.4 h at injection dose of 15 mg/kg b.w. (Fig. 1(A)). Incorporation of as little as 0.3 mol% of PEG-DSPE did not affect the circulation time of SA-Ve. Incorporation of above 0.6 mol% of PEG-DSPE prolonged the circulation time of SA-Ve and the $t_{1/2}$ increased with increasing amounts of PEG-DSPE incorporation as summarized in Table 1. The incorporation of 2.6 mol% of PEG-DSPE also gave a remarkable improvement in circulation time for control Ve ($t_{1/2}$: 24.8 h). At 24 h post injection, the radioactivity of excised organs was counted using a scintillation counter. Major organs exhibiting the uptake of vesicles were bone marrow and liver for SA-Ve (Figs. 1(B) and (C)), while liver and spleen were the organs with the highest accumulation of control Ve (Figs. 1(C) and (D)). PEG modification clearly inhibited hepatic uptake of both SA-Ve and control Ve, and this effect became significant as the amount of PEG-DSPE incorporated increased (Fig. 1(C)). While a maximum amount of SA-Ve was observed in bone marrow when the SA-Ve contained 0.6 mol% PEG-DSPE, further incorporation of PEG-DSPE led to a decrease in the distribution of SA-Ve in bone marrow (Fig. 1(B)). Other organs apart from kidney and muscle for PEG(2.6)-[SA-Ve] exhibited only a small amount of activity (<1%ID, Supplementary Table 1 online). Injection in rabbits of a mixed solution of $^{99\text{m}}\text{Tc}$ -HMPAO and glutathione in a similar ratio as would be found within $^{99\text{m}}\text{Tc}$ -vesicles served as a control study of the radiolabeling agents without encapsulation within the vesicles. As shown in Fig. 2(A), injection of $^{99\text{m}}\text{Tc}$ -HMPAO/glutathione was rapidly eliminated from blood circulation ($t_{1/2}$: 3 min), and gamma camera images indicated that the labeling agents were rapidly excreted in urine through the kidney (Fig. 2(B)). Region of interest analysis showed that $67.1 \pm 0.8\%$ of injected radioactivity was detected in bladder within 1 h after injection (Fig. 2(C)). At 6 h, biodistribution data also showed significant radioactivity in the urine ($76.91 \pm 4.80\%$ ID) and kidney ($6.11 \pm 0.53\%$ ID), but other organs including bone marrow had only minimal %ID dose uptake as summarized in Table 2. This control study shows that a mixture of $^{99\text{m}}\text{Tc}$ -HMPAO and glutathione is rapidly removed from the blood by renal excretion, which is

Table 1
Specification of prepared vesicles

Sample ^a	Mean diameter \pm SD (nm)	PEG-DSPE (mol%)	$t_{1/2}$ (h) ^b
SA-Ve	269 \pm 11	0	0.6
PEG(0.3)-[SA-Ve]	276 \pm 13	0.3	0.6
PEG(0.6)-[SA-Ve]	273 \pm 12	0.6	1.0
PEG(1.4)-[SA-Ve]	275 \pm 12	1.4	3.9
PEG(2.6)-[SA-Ve]	274 \pm 12	2.6	5.4
Ve	262 \pm 43	0	9.4
PEG(2.6)-Ve	259 \pm 74	2.6	24.8

^aSA-Ve is based on DPPC/CH/SA (molar ratio, 1:1:0.2), and Ve is DPPC/CH (molar ratio, 1:1) as a control sample. PEG-modified samples were prepared using the spontaneous incorporation of PEG-DSPE into the prepared SA-Ve or Ve.

^bThe $t_{1/2}$ values were calculated from Fig. 1(A) data.

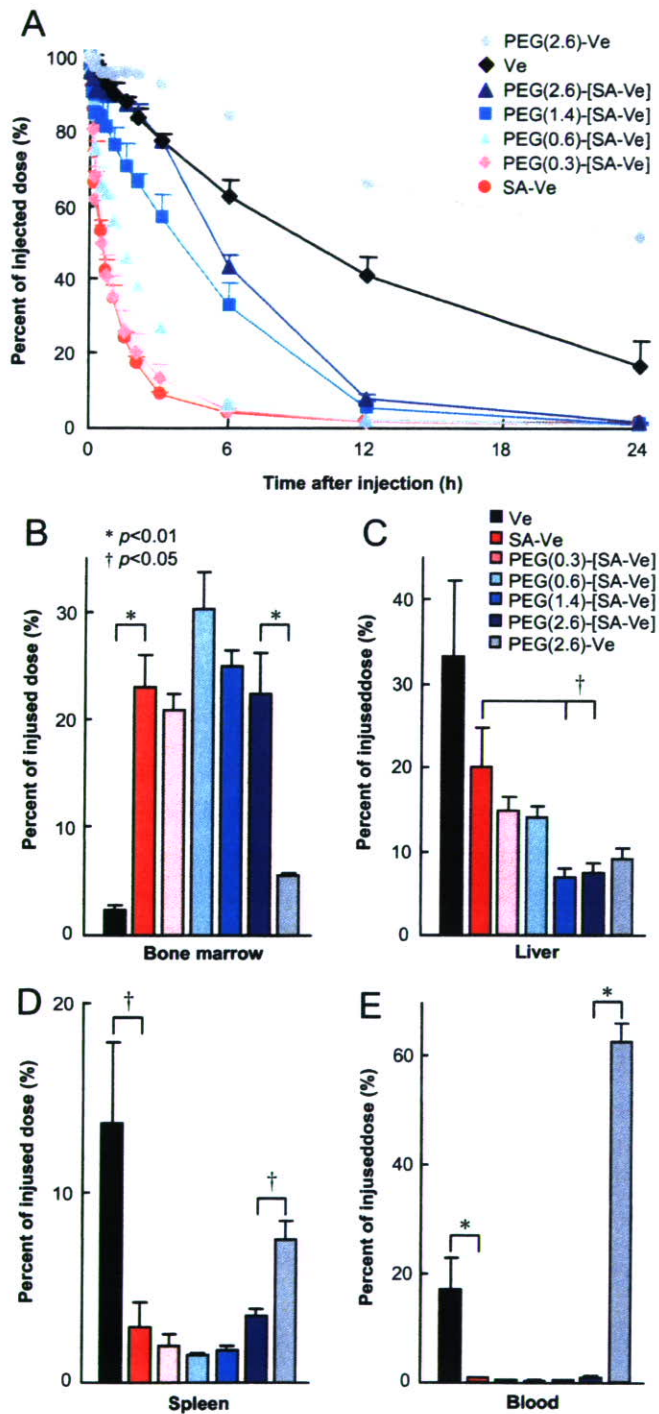


Fig. 1. Effect of surface modification with SA and PEG-DSPE on circulation kinetics and organ distribution of phospholipid vesicles. (A) Circulation kinetics of SA-vesicles (SA-Ve) and control vesicles (Ve) containing various amounts of PEG-DSPE after i.v. infusion (lipids: 15 mg/kg b.w.) in rabbits. ^{99m}Tc radioactivity was quantitated by scintillation counting of blood samples with time. The percentage of injected dose was calculated as a percentage of baseline radioactivity in a blood sample withdrawn just after injection. (B)–(E) Distribution of SA-vesicles (SA-Ve) and control vesicles (Ve) containing various amounts of PEG-DSPE as a percentage of the injected dose in bone marrow (B), liver (C), spleen (D), and blood (E) at 24 h after i.v. infusion in rabbits. *, Statistical significance ($p < 0.01$), †, statistical significance ($p < 0.05$).

typical of small molecules. These results indicate that the SA-Ve were clearly directed to bone marrow, and the process of accumulation of SA-Ve into bone marrow is correlated with competitive trapping by liver. Surface modification of SA-Ve with the proper amount of PEG-lipids inhibits the trapping of SA-Ve in liver and directs SA-Ve to bone marrow, a process which could be regarded as a combination of active and passive targeting. Conventional anionic vesicles containing phosphatidyl glycerol (PG) were inactive for targeting of bone marrow (Supplementary Table 2 online). The injected PEG(0.6)-[SA-Ve], which was the formulation showing the highest persistence in bone marrow at 24 h, were almost removed from circulation within 6 h (as little as $6.4 \pm 0.5\%$ ID of PEG(0.6)-[SA-Ve] was circulating in blood at 6 h). Therefore, the initial distribution kinetics of PEG(0.6)-[SA-Ve] was studied in detail.

3.3. Distribution kinetics of PEG(0.6)-[SA-Ve]

Scintigraphic images clearly showed the injected radioactivity of PEG(0.6)-[SA-Ve] to be redirected from heart and liver, both organs having large blood pool contributions, and increasingly deposited in the bone marrow over time (Fig. 3(A)). The distribution kinetics in bone marrow, liver, and spleen, analyzed from the scintigraphic images, quantitatively indicated that significantly higher doses had accumulated in bone marrow, reaching $68.5 \pm 3.3\%$ ID by 6 h after injection (Fig. 3(B)). The biodistribution data calculated from the radioactivity of excised organs also showed that $69.74 \pm 0.3\%$ ID of PEG(0.6)-[SA-Ve] had accumulated in bone marrow, as shown in Table 2. At the same time point, liver and spleen had much smaller amounts of 11.51 ± 2.88 and $5.00 \pm 1.19\%$ ID, respectively. When ^{99m}Tc -HMPAO/glutathione was injected without encapsulation into PEG(0.6)-[SA-Ve], bone marrow, liver, and spleen had only 1.13 ± 0.24 , 1.52 ± 0.14 , and $0.01 \pm 0.00\%$ ID, respectively. The isolated femur was further separated into soft bone marrow, joint bone (sponge bone), and skeleton and each separate tissue counted for radioactivity. As shown in Fig. 3(C), $66.5 \pm 1.1\%$ of radioactivity in one femur was detected in soft bone marrow. The joint bone including soft bone marrow had $28.8 \pm 1.3\%$ of radioactivity, and less radioactivity was detected in the separated skeleton ($4.7 \pm 0.3\%$). These results indicate that the intravenously injected PEG(0.6)-[SA-Ve] mostly accumulates into soft bone marrow. The gamma camera images clearly show that the bone marrow uptake was evenly distributed over whole bone (Fig. 4), and the localization of radioactivity representing the distribution of PEG(0.6)-[SA-Ve] in these images was analyzed for separate regions. The spine and pelvis had $21.23 \pm 0.42\%$ and $18.09 \pm 0.60\%$, values which were much higher than other regions. The right and left femurs had equal radioactivity of $7.97 \pm 0.05\%$ and $8.34 \pm 0.18\%$; these values are in agreement with a report

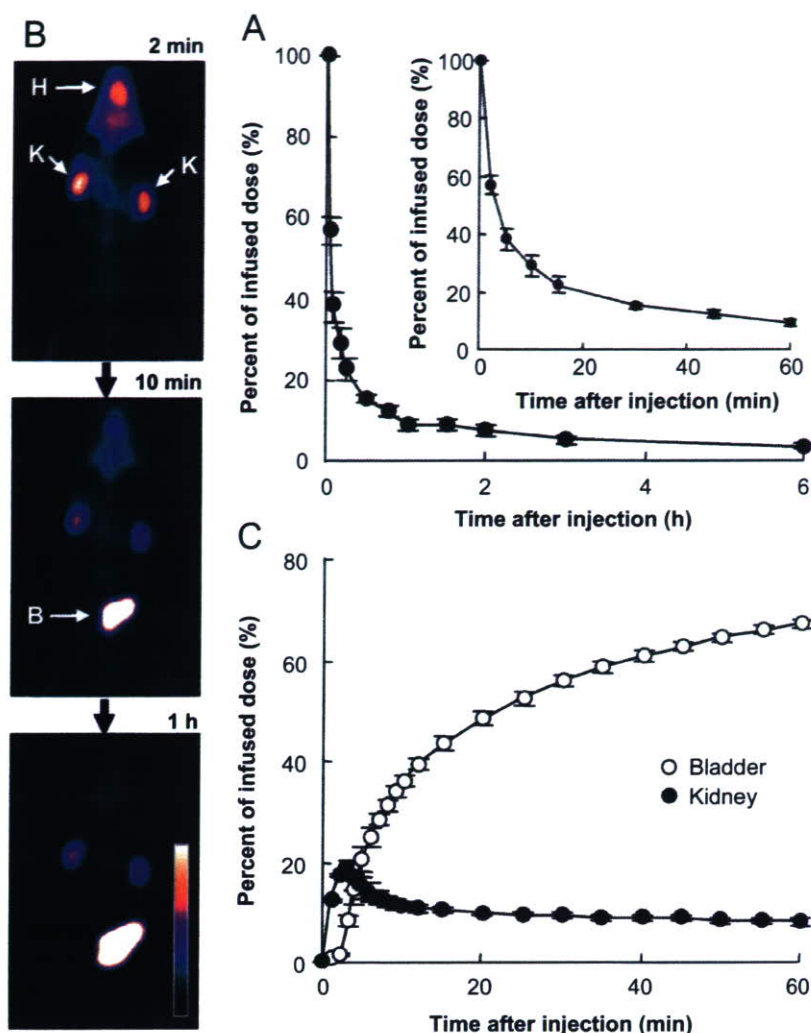


Fig. 2. Circulation and distribution kinetics of mixture of ^{99m}Tc -HMPAO and glutathione without encapsulation in vesicles after i.v. infusion in rabbits. (A) Circulation kinetics (B) Gamma camera images of rabbits acquired at various times after infusion. H: heart, K: kidney, B: bladder. (C) Distribution profiles as a percentage of the injected dose analyzed from the gamma camera images.

describing the relationship of 12 times that of a femur as being equivalent to whole bone in rabbits [28].

3.4. Microscopic localization of PEG(0.6)-[SA-Ve] in bone marrow

The initial studies were designed to demonstrate that PEG(0.6)-[SA-Ve] functions as a nanoparticulate carrier as well as identify their microscopic localization in tissues. We used PEG(0.6)-[SA-Ve] double-labeled by encapsulating water-soluble TR-SOD in an aqueous phase and embedding lipid-soluble C_1 -BODIPY C_{12} in bilayer membrane (Fig. 5(A)). As shown in Fig. 5(B), the bone marrow sections have fluorescence from both the TR-SOD and C_1 -BODIPY C_{12} . The fluorescence was locally concentrated, and larger fluorescent domain was 30 μm in size along the long axis. Fluorescent distribution in red pulp of spleen was dense, whereas it was sparse in liver. An important

finding from this observation is that the fluorescence from membrane probes and encapsulated probes are co-localized in bone marrow. These images clearly indicate that PEG(0.6)-[SA-Ve] functions as a nanoparticle-carrier to deliver the encapsulated agents to bone marrow tissues. A second study was performed to identify the histological location of PEG(0.6)-[SA-Ve] in bone marrow. Femoral bone marrow tissue was taken from rabbit at 6 h after i.v. injection of PEG(0.6)-[SA-Ve] and examined using TEM. TEM observation clearly demonstrated the location of PEG(0.6)-[SA-Ve] in bone marrow (Figs. 6(A) and (B)). A massive number of vesicles were trapped in endosomes and lysosomes of BMM ϕ , but no vesicles were observed in cytoplasm and cell nucleus (Fig. 6(B)). The diameter of these vesicles averaged 270 nm which was the original diameter of the intravenously administered PEG(0.6)-[SA-Ve]. Several similar BMM ϕ with vesicles in endosomes and lysosomes were observed, while no vesicles were observed

Table 2

Biodistribution of PEG(0.6)-[SA-Ve] and ^{99m}Tc -HMPAO/glutathione as a percent of the injected dose (%ID) and %ID per gram of tissue at 6 h after i.v. infusion in rabbits

Organs	PEG(0.6)-[SA-Ve]		^{99m}Tc -HMPAO/glutathione	
	%ID \pm SEM (%)	%ID/g tissue \pm SEM (%/g)	%ID \pm SEM (%)	%ID/g tissue \pm SEM (%/g)
Blood	6.58 \pm 2.91	0.065 \pm 0.028	3.34 \pm 1.68	0.025 \pm 0.013
Bone marrow	69.74 \pm 0.86	0.806 \pm 0.048	1.13 \pm 0.24	0.010 \pm 0.001
Liver	11.51 \pm 2.88	0.237 \pm 0.067	1.52 \pm 0.14	0.022 \pm 0.001
Spleen	5.00 \pm 1.19	5.387 \pm 0.807	0.01 \pm 0.00	0.011 \pm 0.001
Bowel	5.85 \pm 0.31	0.014 \pm 0.000	4.41 \pm 0.19	0.009 \pm 0.000
Skin	1.57 \pm 0.21	0.009 \pm 0.001	2.34 \pm 0.30	0.010 \pm 0.001
Kidney	2.40 \pm 0.10	0.148 \pm 0.011	6.11 \pm 0.53	0.440 \pm 0.066
Muscle	1.86 \pm 0.17	0.003 \pm 0.000	2.60 \pm 0.63	0.002 \pm 0.001
Lung	0.19 \pm 0.03	0.024 \pm 0.006	0.12 \pm 0.03	0.010 \pm 0.001
Heart	0.03 \pm 0.01	0.010 \pm 0.002	0.03 \pm 0.01	0.006 \pm 0.001
Brain	0.01 \pm 0.00	0.002 \pm 0.000	0.01 \pm 0.00	0.001 \pm 0.000
Testis	0.03 \pm 0.01	0.024 \pm 0.005	0.02 \pm 0.00	0.008 \pm 0.002
Urine	3.57 \pm 1.74	—	76.91 \pm 4.80	—

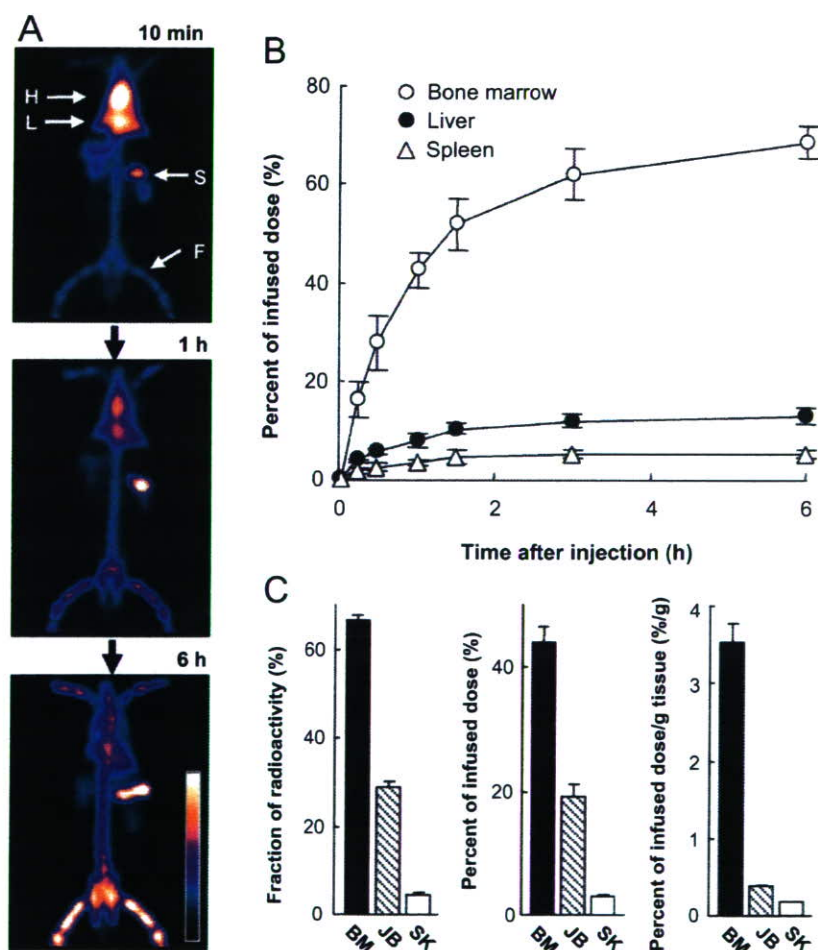


Fig. 3. Initial distribution kinetics of PEG(0.6)-[SA-Ve] after i.v. infusion (lipids: 15 mg/kg b.w.) in rabbits. (A) Gamma camera images of rabbits acquired at various times after infusion. H: heart, L: liver, S: spleen, F: femur. (B) Distribution profiles as a percentage of the injected dose analyzed from the gamma camera images. The total bone marrow was estimated to be 12 times that of one femur. (C) Distribution of radioactivity of PEG(0.6)-[SA-Ve] in separated soft bone marrow (BM), joint bone (sponge bone) (JB), and skeleton (SK) of one femur collected at 6 h after i.v. infusion. Three panels show the fraction of radioactivity, percent of injected dose (%ID), and %ID/g tissue, respectively.

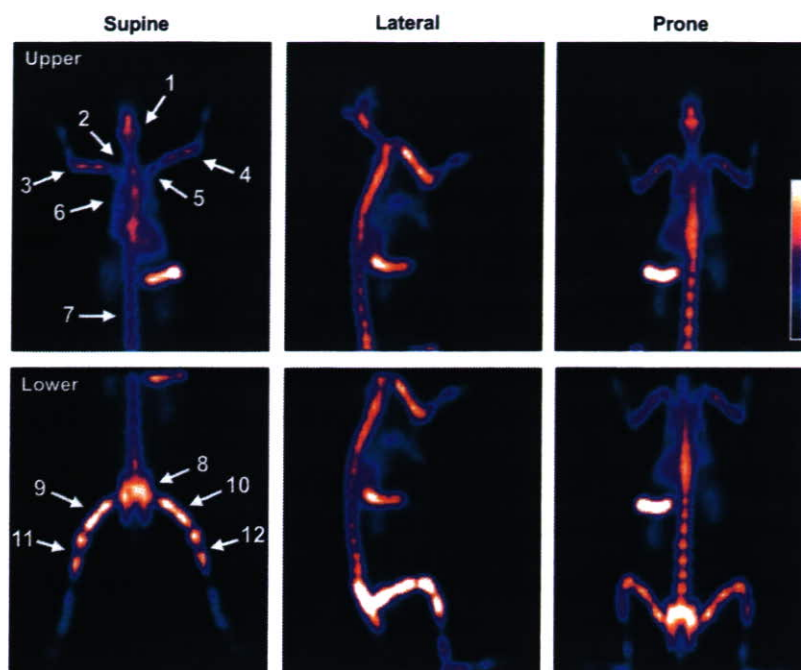


Fig. 4. Gamma camera images of rabbit receiving PEG(0.6)-[SA-Ve], acquired from various angles at 6 h after i.v. infusion. Bone marrow is clearly displayed in these images throughout the rabbit body. Relative radioactivity in separated bone parts were calculated to 1; head ($8.41 \pm 1.58\%$), 2; neck ($1.10 \pm 0.11\%$), 3; right arm ($5.72 \pm 0.33\%$), 4; left arm ($5.54 \pm 0.40\%$), 5; shoulder ($3.62 \pm 0.69\%$), 6; sternum ($4.11 \pm 1.35\%$), 7; spine ($21.23 \pm 0.42\%$), 8; pelvis ($18.09 \pm 0.60\%$), 9; right femur ($7.97 \pm 0.05\%$), 10; left femur ($8.34 \pm 0.18\%$), 11; distal right foot ($7.88 \pm 0.25\%$), and 12; distal left foot ($7.98 \pm 0.33\%$) as percentages to radioactivity of whole bone \pm SEM.

in other types of cell such as granular leukocytes, erythroblasts, and endothelial cells in observed section. These microscopic localization studies demonstrate that BMM ϕ are the cellular components responsible for clearance of vesicles from the circulation and their uptake by the bone marrow.

4. Discussion

These studies demonstrate that PEG-[SA-Ve] are efficient carriers for targeting the BMM ϕ . These vesicles should be useful in the development of bone marrow targeted agents for therapeutic applications. Additionally, this *in vivo* model appears to be an ideal model with which to investigate the role of BMM ϕ in the hematopoietic environment. The radiolabeling method for the vesicles encapsulating glutathione with ^{99m}Tc -HMPAO has previously been established for imaging studies [14,23,24]. In the present vesicle formulation, we confirmed the stability of the ^{99m}Tc radiolabeled-vesicles during incubation in serum and plasma at 37°C for 48 h (more than 95% remaining with vesicles), and we also determined that the free labeling agent is not specifically distributed into organs such as bone marrow, liver, and spleen, but rapidly eliminated through renal excretion as shown in Fig. 2 and Table 2. This evidence provides strong support that the radioisotope distribution reflects the true biodistribution of vesicles. As shown in Fig. 1, comparative data showing the organ distribution of several formulations clearly demon-

strated that the uptake of vesicles by bone marrow is induced by the incorporation of SA ($p < 0.01$); furthermore, the incorporation of a small amount of PEG-DSPE on the surface of SA-Ve prolongs its circulation time and tends to enhance the bone marrow selectivity by preventing hepatic uptake. Thus, maximum distribution to bone marrow was observed at 0.6 mol% PEG-DSPE (Fig. 1(B)). The degree of hepatic uptake was reduced as the PEG-DSPE content increased, and this effect became significant above 1.4 mol% ($p < 0.05$). Bone marrow uptake was also reduced above 1.4 mol%. In general, 5–10 mol% of PEG-lipids is incorporated into most of the long circulating vesicle formulations for passive targeting [8,9]. In the present study, prolonged circulation time of vesicles was observed above 0.6 mol% of PEG-DSPE, and the circulation times were prolonged more in vesicles with higher PEG-DSPE content. For the effective targeting of bone marrow, however, higher concentrations of PEG blocked the active targeting of the vesicles to bone marrow. These results indicate that the dense PEG layer on the vesicular surface covers the surface properties having the character of SA and depress uptake by BMM ϕ . Therefore, the optimal amount of PEG incorporation was found to be 0.6 mol%, as this concentration passively enhances active targeting. Theoretically, approximately 0.4 mol% of PEG (Mw 5000)-lipids is estimated to be the critical content required to fully cover the vesicle surface which consists of DPPC and CH (1:1 molar ratio) with the mushroom conformation of PEG chains from Eqs. (1) to (3). Thus, it is

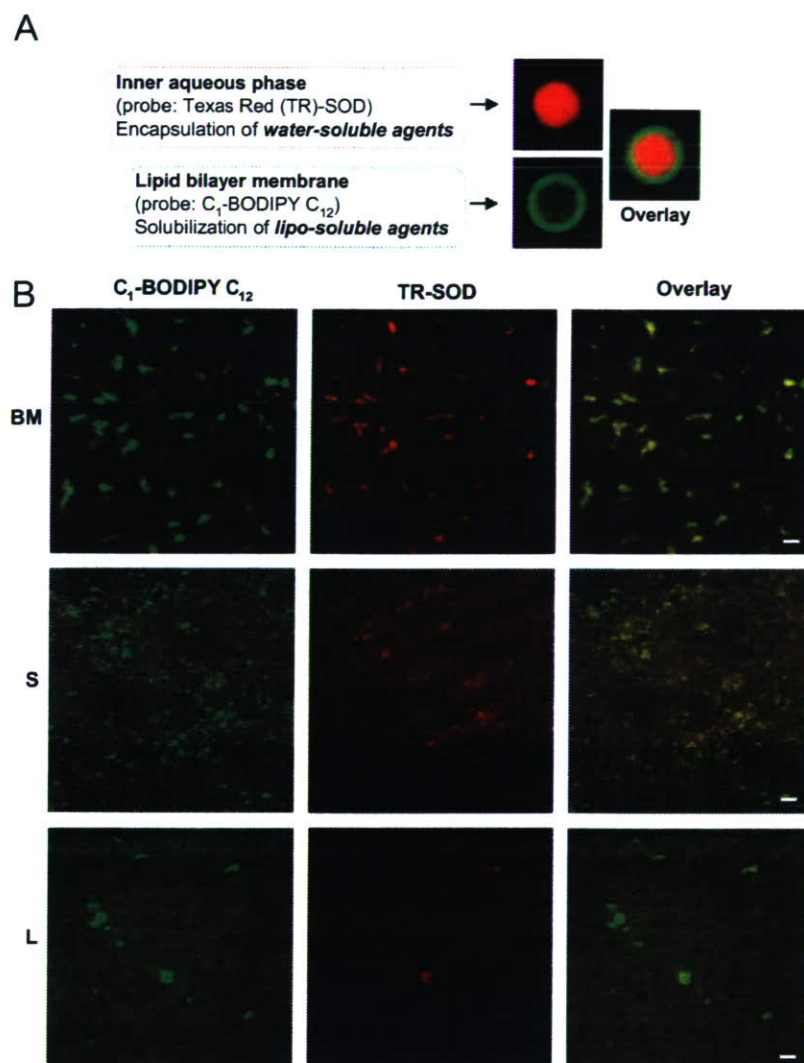


Fig. 5. Histological examination of fluorescence delivered into bone marrow tissues using PEG(0.6)-[SA-Ve] as carriers. (A) Fluorescence localization in double fluorescence-labeled large multilamellar PEG(0.6)-[SA-Ve] with diameter of ca. 10 μm . This observation was performed before extrusion to submicron size to enable observation of the structure within resolution of a confocal microscope. This image indicates that red fluorescence comes from TR-SOD which is encapsulated in inner aqueous phase and green fluorescence comes from C₁-BODIPY C₁₂ which is embedded in bilayer membrane. (B) Confocal scanning images of femoral bone marrow (BM), spleen (S), and liver (L) taken from rabbit at 6 h after i.v. injection of double fluorescence-labeled PEG(0.6)-[SA-Ve] with size of 247 ± 22 nm in diameter (lipids: 15 mg/kg b.w.). The scale bars represent 20 μm .

estimated that the optimal incorporation amount of PEG-lipids is slightly higher than that required to fully cover the vesicular surface. This finding provides useful information for the design of vesicle surface to passively enhance the active targeting with PEG-modification *in vivo*.

To examine the participation of the anionic properties of vesicles in BMM ϕ uptake, we investigated the organ distribution of conventional anionic vesicles containing PG with same protocol. These PG-vesicles do not distribute to the bone marrow (Supplementary Table 2 online, only $5.36 \pm 0.65\%$ ID of PG-vesicles were taken up by the bone marrow at 24 h after i.v. injection). Comparative data for Ve and SA-Ve are shown in Fig. 1(B) and Supplementary Table 1. Previous publications have also supported the observation that PG-vesicles do not distribute to the bone

marrow [33], and neutral vesicles with various sizes in the range of 136.2–318 nm do not distribute to the bone marrow [34]. These results indicated that the targeting of bone marrow is not general for neutral vesicles and is achieved not only by the anionic surface of vesicles. The results suggest that SA is specifically responsible for the bone marrow targeting.

Histological observations showed that the vesicles and encapsulated agents are distributed at the same locations into bone marrow tissues, clearly indicating that the encapsulated agents were delivered to the bone marrow tissues by the vesicles (Fig. 5). Higher magnification TEM observations have demonstrated that a massive number of vesicles are trapped in the endosomes and lysosomes of the BMM ϕ (Fig. 6). These observations indicated that the

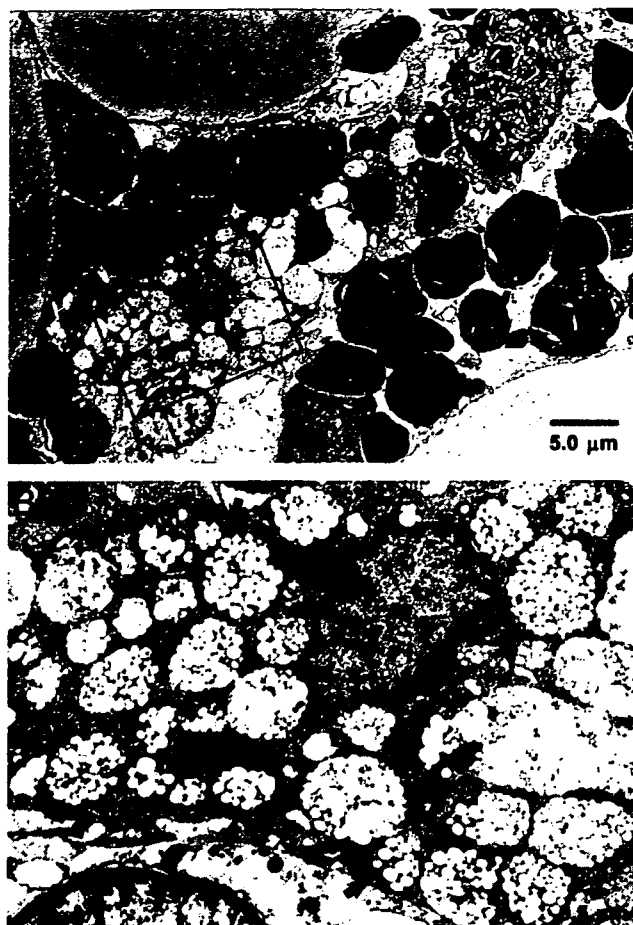


Fig. 6. Transmission electron micrographs of femoral bone marrow tissue section, taken from rabbit at 6 h after i.v. injection of PEG(0.6)-[SA-Ve] (lipids: 15 mg/kg b.w.). (A) Low magnified micrograph representing the bone marrow tissue including macrophage and various bone marrow cells. (B) High magnified micrograph of framed region in panel (A). A massive number of vesicles with original diameter (average 270 nm) are trapped in several endosomes or lysosomes of macrophage. Some are indicated by arrows, which shows same position in (A) and (B).

uptake of PEG(0.6)-[SA-Ve] by bone marrow was responded by the endocytosis of BMM ϕ . One potent trigger to accelerate the cellular endocytosis for vesicles is an interaction with the receptors on the surface of cells, that are known as a receptor-mediated endocytosis which is investigated as a potent pathway for drug targeting to specific cell including macrophage [2,10,11]. Scavenger receptors are membrane glycoproteins that are present mainly on cells of the macrophage lineage [35,36]. Various polyanionic compounds such as dextran sulfate, polyinosinic acid, and acetylated low density lipoproteins have been reported as ligands for this receptor [37,38]. These compounds are taken at high levels by macrophages via a scavenger receptor-mediated mechanism. On the other hand, many polyanions such as chondroitin sulfate, poly(D-glutamic) acid, and polycytidylic acid are not ligands for scavenger receptors [37,38]. Previous investigations indi-

cated that the scavenger receptors on macrophages contribute to the recognition of polyanionic structures, resulting in selective uptake. Enhanced uptake of succinylated proteins has been investigated in cultured brain microvessel endothelial cells. Endothelial cells also express the scavenger receptor on their surface. Large succinylated proteins such as catalase (Mw 227 kDa) and bovine serum albumin (Mw 70 kDa) were taken up by the cells via a scavenger receptor-mediated mechanism, whereas significant uptake was not observed for native proteins and small succinylated proteins such as SOD (Mw 34 kDa) and soybean trypsin inhibitor (Mw 21 kDa) [39]. This indicates that succinylation of large molecules is involved in the uptake via a scavenger receptor-mediated mechanism. Recently, Szabó et al. reported the uptake of branched polypeptides by bone marrow culture-derived murine macrophages. They indicated that the succinylation of branched polypeptides significantly enhanced the uptake by macrophages, and the uptake was inhibited by blocking of the class-A scavenger receptors [40]. Because the terminal hydrophilic head group of SA is corresponding to the succinylated structure, we speculate that the interaction between PEG-[SA-Ve] and the scavenger receptors on BMM ϕ might participate in the selective uptake. However, further mechanistic investigation on uptake of PEG-[SA-Ve] by BMM ϕ , splenic macrophages, and hepatic Kupffer cells is necessary to clarify the mechanism of organ selective macrophage uptake.

Previous pharmacokinetic studies have been performed using vesicles containing SA that have the same lipid composition as in the present study with PEG(0.3)-[SA-Ve], but a significantly higher dose was employed (lipids: 680 mg/kg b.w.) [17]. In these studies, the bone marrow-selective distribution was not observed, so it appears that the bone marrow selectivity is limited by the injection dosage in certain applications. As the vesicle dosage increases, the MPS in the bone marrow becomes saturated; as a result, liver and spleen uptake is increased. In our previous organ distribution study in rabbits, >50%ID of the vesicles were still in circulation at 48 h after infusion of a massive dose of vesicles, while the bone marrow had $7.36 \pm 0.34\%$ of 680 mg/kg b.w. at the same time point [17]. This value is equivalent to 50.0 mg/kg b.w., and it can be used to estimate the maximum uptake capacity of MPS for vesicles. When vesicle dosage increases above 50.0 mg/kg b.w., the bone marrow is the first organ to become saturated, and the accumulation of vesicles then increases in the liver and spleen. Such sequential saturation of the MPS eliminates organ selectivity. Therefore, the bone marrow targeting of SA-Ve becomes striking when the dose of vesicles is below the saturation dosage for bone marrow, as observed in the present study (15 mg/kg b.w.). The ability of vesicular nanoparticles to encapsulate a wide variety of agents provides significant opportunities for bone marrow delivery applications. In the present study, we have demonstrated the delivery of scintigraphic and fluorescence imaging agents to bone marrow by using the

SA-Ve vesicles. This method has advantages in delivering the therapeutic agents to treat bone marrow disorders.

5. Conclusion

This is the first report to show the organ distribution of PEG-[SA-Ve] at small dose injection. Organ distributions of several vesicular formulations were quantitatively compared to determine the component to induce the significant distribution into bone marrow. Our data have indicated that surface modification of phospholipid vesicles with two compounds, SA and PEG-DSPE, cooperatively induces the significant bone marrow targeting properties to vesicles. In this system, BMM ϕ participated in the uptake of PEG-[SA-Ve], and the efficient delivery of the vesicles as encapsulating agents into the bone marrow was achieved within 6 h after injection. These results indicated that the PEG-[SA-Ve] is a potent carrier for drug delivery into BMM ϕ *in vivo* and may be useful for delivering a wide range of therapeutic agents to bone marrow.

Acknowledgments

This work was partly supported by project of a Health and Labor Sciences Research Grant (Research on Pharmaceutical and Medical Safety, Artificial Blood Project) of the Ministry of Health, Labor and Welfare, Japan, and the Ministry of Education, Culture, Sports, Science and Technology, Grant-in-Aid for Scientific Research (B), 17300162, 2005. The authors gratefully acknowledge Dr. H. Sakai (Waseda University) for discussions on this research, Dr. Linda M. McManus (UTHSCSA) for assistance with electron microscopic images and Mr. R. Klipper (UTHSCSA) for technical support.

Appendix A. Supplementary materials

The online version of this article contains additional supplementary data. Please visit doi:10.1016/j.biomaterials.2007.01.041.

References

- [1] Farokhzad OD, Jon S, Khademhosseini A, Tran TN, Lavan DA, Langer R. Nanoparticle–aptamer bioconjugates: a new approach for targeting prostate cancer cells. *Cancer Res* 2004;64:7668–72.
- [2] Torchilin VP. Recent advances with liposomes as pharmaceutical carriers. *Nat Rev Drug Discov* 2005;4:145–60.
- [3] Gregoriadis G, Wills EJ, Swain CP, Tavill AS. Drug-carrier potential of liposomes in cancer chemotherapy. *Lancet* 1974;1:1313–6.
- [4] Felgner PL, Gadek TR, Holm M, Roman R, Chan HW, Wenz M, et al. Lipofection: a highly efficient, lipid-mediated DNA-transfection procedure. *Proc Natl Acad Sci USA* 1987;84:7413–7.
- [5] Moghimi SM, Hunter AC, Murray JC. Long-circulating and target-specific nanoparticles: theory to practice. *Pharmacol Rev* 2001;53:283–318.
- [6] Sakai H, Horinouchi H, Tomiyama K, Ikeda E, Takeoka S, Kobayashi K, et al. Hemoglobin-vesicles as oxygen carriers: influence on phagocytic activity and histopathological changes in reticuloendothelial system. *Am J Pathol* 2001;159:1079–88.
- [7] Fadok VA, Bratton DL, Rose DM, Pearson A, Ezekewitz RA, Henson PM. A receptor for phosphatidylserine-specific clearance of apoptotic cells. *Nature* 2000;405:85–90.
- [8] Klivanov AL, Maruyama K, Torchilin VP, Huang L. Amphipathic polyethyleneglycols effectively prolong the circulation time of liposomes. *FEBS Lett* 1990;268:235–7.
- [9] Gabizon A, Shmeeda H, Barenholz B. Pharmacokinetics of pegylated liposomal Doxorubicin: review of animal and human studies. *Clin Pharmacokinet* 2003;42:419–36.
- [10] Turk MJ, Water DJ, Low PS. Folate-conjugated liposomes preferentially target macrophages associated with ovarian carcinoma macrophage. *Cancer Lett* 2004;213:165–72.
- [11] Chellat F, Merhi Y, Moreau A, Yahia L'H. Therapeutic potential of nanoparticulate systems for macrophage targeting. *Biomaterials* 2005;26:7260–75.
- [12] Mantovani A, Sozzani S, Locati M, Allavena P, Sica A. Macrophage polarization: tumor-associated macrophages as a paradigm for polarized M2 mononuclear phagocytes. *Trends Immunol* 2002;23:549–55.
- [13] Allen TM, Austin GA, Chonn A, Lin L, Lee KC. Uptake of liposomes by cultured mouse bone marrow macrophages: influence of liposome composition and size. *Biochim Biophys Acta* 1991;1061:56–64.
- [14] Phillips WT, Klipper RW, Awasthi VD, Rudolph AS, Cliff R, Kwasiborski V, et al. Polyethylene glycol-modified liposome-encapsulated hemoglobin: a long circulating red cell substitute. *J Pharmacol Exp Ther* 1999;288:665–70.
- [15] Dams ET, Oyen WJ, Boerman OC, Storm G, Laverman P, Kok PJ, et al. ^{99m}Tc-PEG liposomes for the scintigraphic detection of infection and inflammation: clinical evaluation. *J Nucl Med* 2000;41:622–30.
- [16] Giuliani AL, Wiener E, Lee MJ, Brown IN, Berti G, Wickramasinghe SN. Changes in murine bone marrow macrophages and erythroid burst-forming cells following the intravenous injection of liposome-encapsulated dichloromethylene diphosphonate (Cl₂MDP). *Eur J Haematol* 2001;66:221–9.
- [17] Sou K, Klipper R, Goins B, Tsuchida E, Phillips WT. Circulation kinetics and organ distribution of Hb-vesicles developed as a red blood cell substitute. *J Pharmacol Exp Ther* 2005;312:702–9.
- [18] Sadahira Y, Mori M. Role of the macrophage in erythropoiesis. *Pathol Int* 1999;49:841–8.
- [19] Yoshida H, Kawane K, Koike M, Mori Y, Uchiyama Y, Nagata S. Phosphatidylserine-dependent engulfment by macrophages of nuclei from erythroid precursor cells. *Nature* 2005;437:754–8.
- [20] Sou K, Naito Y, Endo T, Takeoka S, Tsuchida E. Effective encapsulation of proteins into size-controlled phospholipid vesicles using freeze-thawing and extrusion. *Biotechnol Prog* 2003;19:1547–52.
- [21] Sou K, Endo T, Takeoka S, Tsuchida E. Poly(ethylene glycol)-modification of the phospholipid vesicles by using the spontaneous incorporation of poly(ethylene glycol)-lipid into the vesicles. *Bioconjug Chem* 2000;11:372–9.
- [22] Sakai H, Hisamoto S, Fukutomi I, Sou K, Takeoka S, Tsuchida E. Detection of lipopolysaccharide in hemoglobin-vesicles by Limulus amoebocyte lysate test with kinetic-turbidimetric gel clotting analysis and pretreatment of surfactant. *J Pharm Sci* 2004;93:310–21.
- [23] Rudolph AS, Klipper R, Goins B, Phillips WT. *In vivo* biodistribution of a radiolabeled blood substitute: ^{99m}Tc-labeled liposome-encapsulated hemoglobin in an anesthetized rabbit. *Proc Natl Acad Sci USA* 1991;88:10976–80.
- [24] Phillips WT, Rudolph AS, Goins B, Timmons JH, Klipper R, Blumhardt R. A simple method for producing a technetium-99m-labeled liposome which is stable *in vivo*. *Nucl Med Biol* 1992;19:539–47.

- [25] Awasthi V, Goins B, Klipper R, Lored R, Korvick D, Phillips WT. Dual radiolabeled liposomes: biodistribution studies and localization of focal sites of infection in rats. *Nucl Med Biol* 1998;25:155–60.
- [26] Kozma C, Macklin W, Cummins LM, Mauer R. Anatomy, physiology, and biochemistry of the rabbit. In: Weisbroth SH, Flatt RE, Kraus AL, editors. *The biology of the laboratory rabbit*. New York: Academic Press; 1974. p. 50–69.
- [27] Kaplan HM, Timmons EH. *The rabbit: a model for the principles of mammalian physiology and surgery*. New York: Academic Press; 1979.
- [28] Deitz AA. Distribution of bone marrow, bone and bone ash in rabbits. *Proc Soc Exp Med* 1944;57:60–2.
- [29] Lefevre C, Kang HC, Haugland RP, Malekzadeh N, Arttamangkul S, Haugland RP. Texas Red-X and rhodamine Red-X, new derivatives of sulforhodamine 101 and lissamine rhodamine B with improved labeling and fluorescence properties. *Bioconjug Chem* 1996;7:482–9.
- [30] Torchilin VP, Papisov MI. Why do polyethylene glycol-coated liposomes circulate so long? *J Liposome Res* 1994;4:725–39.
- [31] Du H, Chandaroy P, Hui SW. Grafted poly-(ethylene glycol) on lipid surface inhibits protein adsorption and cell adhesion. *Biochim Biophys Acta* 1997;1326:236–48.
- [32] Edholm O, Nagle JF. Areas of molecules in membranes consisting mixtures. *Biophys J* 2005;89:1827–32.
- [33] Awasthi VD, Garcia D, Klipper R, Goins BA, Phillips WT. Neutral and anionic liposome-encapsulated hemoglobin: effect of postinserted poly(ethylene glycol)-distearoylphosphatidylethanolamine on distribution and circulation kinetics. *J Pharmacol Exp Ther* 2004;309:241–8.
- [34] Awasthi VD, Garcia D, Goins BA, Phillips WT. Circulation and biodistribution profiles of long-circulating PEG-liposomes of various sizes in rabbits. *Int J Pharm* 2003;253:121–32.
- [35] Doi T, Higashino K, Kurihara Y, Wada Y, Miyazaki T, Nakamura H, et al. Charged collagen structure mediates the recognition of negatively charged macromolecules by macrophage scavenger receptors. *J Biol Chem* 1993;268:2126–33.
- [36] Taylor PR, Martinez-Pomares L, Stacey M, Lin HH, Brown GD, Gordon S. Macrophage receptors and immune recognition. *Annu Rev Immunol* 2005;23:901–44.
- [37] Brown MS, Goldstein JL. Lipoprotein metabolism in the macrophage: implications for cholesterol deposition in atherosclerosis. *Annu Rev Biochem* 1983;52:223–61.
- [38] Krieger M, Acton S, Ashkenas J, Pearson A, Penman M, Resnick D. Molecular flypaper, host defense, and atherosclerosis. Structure, binding properties, and functions of macrophage scavenger receptors. *J Biol Chem* 1993;268:4569–72.
- [39] Tokuda H, Masuda S, Takakura Y, Sezaki H, Hashida M. Specific uptake of succinylated proteins via a scavenger receptor-mediated mechanism in cultured brain microvessel endothelial cells. *Biochem Biophys Res Commun* 1993;196:18–24.
- [40] Szabó R, Peiser L, Plüddemann A, Bösze S, Heinsbroek S, Gordon S, et al. Uptake of branched polypeptides with poly[L-lys] backbone by bone-marrow culture-derived murine macrophages: the role of the class A scavenger receptor. *Bioconjug Chem* 2005;16:1442–50.

Rheological Properties of Hemoglobin Vesicles (Artificial Oxygen Carriers) Suspended in a Series of Plasma-Substitute Solutions

Hiromi Sakai,[†] Atsushi Sato,[‡] Shinji Takeoka,[‡] and Eishun Tsuchida^{*†}

Advanced Research Institute for Science and Engineering and Graduate School of Science and Engineering, Waseda University, Tokyo 169-8555, Japan

Received February 15, 2007. In Final Form: April 3, 2007

Hemoglobin vesicles (HbV) or liposome-encapsulated Hbs are artificial oxygen carriers that have been developed for use as transfusion alternatives. The extremely high concentration of the HbV suspension (solute, ca. 16 g/dL; volume fraction, ca. 40 vol %) gives it an oxygen-carrying capacity that is comparable to that of blood. The HbV suspension does not possess a colloid osmotic pressure. Therefore, HbV must be suspended in or co-injected with an aqueous solution of a plasma substitute (water-soluble polymer), which might interact with HbV. This article describes our study of the rheological properties of HbV suspended in a series of plasma substitute solutions of various molecular weights: recombinant human serum albumin (rHSA), dextran (DEX), modified fluid gelatin (MFG), and hydroxyethyl starch (HES). The HbV suspended in rHSA was nearly Newtonian. Other polymers—HES, DEX, and MFG—induced HbV flocculation, possibly by depletion interaction, and rendered the suspensions as non-Newtonian with a shear-thinning profile (10^{-4} – 10^3 s⁻¹). These HbV suspensions showed a high storage modulus (G') because of the presence of flocculated HbV. However, HbV suspended in rHSA exhibited a very low G' . The viscosities of HbV suspended in DEX, MFG, and high-molecular-weight HES solutions responded quickly to rapid step changes in shear rates of 0.1–100 s⁻¹ and a return to 0.1 s⁻¹, indicating that flocculation is both rapid and reversible. Microscopically, the flow pattern of the flocculated HbV that perfused through microchannels (4.5 μ m deep, 7 μ m wide, 20 cmH₂O applied pressure) showed no plugging. Furthermore, the time required for passage was simply proportional to the viscosity. Collectively, the HbV suspension viscosity was influenced by the presence of plasma substitutes. The HbV suspension provides a unique opportunity to manipulate rheological properties for various clinical applications in addition to its use as a transfusion alternative.

Introduction

Phospholipid vesicles or liposomes encapsulating or embedding functional drugs or biological materials have been investigated aggressively for use in drug-delivery systems; some were subsequently approved for antifungal or anticancer therapy.¹ Hemoglobin vesicles (HbV) are artificial oxygen carriers that encapsulate a concentrated Hb solution in phospholipid vesicles (280 nm particle diameter).^{2–6} Their oxygen-carrying capacity and safety as a transfusion alternative have been evaluated energetically in animal tests aimed at clinical applications. In contrast to conventional liposomal products, the concentration of the HbV suspension must be extremely high (Hb, 10 g/dL; lipids, 5–6 g/dL); one injection as a transfusion alternative causes the substitution of a large volume of blood: about 40% of the circulating blood volume.⁷ Accordingly, it is important to evaluate its safety not only in terms of the biocompatibility of the HbV particles themselves but also in terms of the rheological property of the HbV suspension, the infusion fluid, compared to the blood hemorheology.^{8–10}

Albumin, dissolved in a blood plasma at ca. 5 g/dL, provides sufficient colloid osmotic pressure (COP, ca. 20 Torr) to play an important role in equilibrating COP between blood and interstitial fluid, thereby maintaining the overall blood volume. This COP is one requisite for a transfusion alternative to sustain blood circulation for transporting oxygen and metabolites. One HbV contains about 30 000 Hb molecules. Therefore, an HbV suspension shows no COP in an aqueous solution. Accordingly, HbV must be suspended in or co-injected with a plasma substitute solution. This requirement is identical to that for emulsified perfluorocarbon, which does not possess COP;^{11,12} it contrasts with characteristics of other Hb-based oxygen carriers (HBOCs), intramolecular cross-linked Hbs, polymerized Hbs, and polymer-conjugated Hbs, which all possess very high COP as protein solutions.^{13–15}

Animal tests of HbV suspended in plasma-derived human serum albumin (HSA) or recombinant HSA (rHSA) showed an oxygen-transporting capacity that is comparable to that of

* To whom correspondence should be addressed. E-mail: eishun@waseda.jp. Tel: +81-3-5286-3120. Fax: +81-3-3205-4740.

[†] Advanced Research Institute for Science and Engineering.

[‡] Graduate School of Science and Engineering.

(1) Torchilin, V. P. *Nat. Rev. Drug Discovery* **2005**, *4*, 145–160.
(2) Izumi, Y.; Sakai, H.; Hamada, K.; Takeoka, S.; Yamahata, T.; Kato, R.; Nishide, H.; Tsuchida, E.; Kobayashi, K. *Crit. Care Med.* **1996**, *24*, 1869–1873.
(3) Sakai, H.; Takeoka, S.; Park, S. I.; Kose, T.; Nishide, H.; Izumi, Y.; Yoshizu, A.; Kobayashi, K.; Tsuchida, E. *Bioconjugate Chem.* **1997**, *8*, 23–30.
(4) Chang, T. M. *Artif. Organs* **2004**, *28*, 789–794.
(5) Djordjevic, L.; Miller, I. F. *Exp. Hematol.* **1980**, *8*, 584–592.
(6) Phillips, W. T.; Klipper, R. W.; Awasthi, V. D.; Rudolph, A. S.; Cliff, R.; Kwasiborski, V.; Goins, B. A. *J. Pharmacol. Exp. Ther.* **1999**, *288*, 665–670.
(7) Sakai, H.; Horinouchi, H.; Yamamoto, M.; Ikeda, E.; Takeoka, S.; Takaori, M.; Tsuchida, E.; Kobayashi, K. *Transfusion* **2006**, *46*, 339–347.

(8) Makino, C.; Kimura, N.; Hasegawa, E.; Tsuchida, E. *Nippon Kagaku Kaishi* **1991**, *8*, 1102–1105.

(9) Sakai, H.; Hamada, K.; Takeoka, S.; Nishide, H.; Tsuchida, E. *Biotechnol. Prog.* **1996**, *12*, 119–125.

(10) Chung, T. W.; Huang, Y. Y.; Wu, C. I. *Artif. Cells, Blood Substitutes, Immobilization Biotechnol.* **1999**, *27*, 215–227.

(11) Nolte, D.; Pickelmann, S.; Lang, M.; Keipert, P.; Messmer, K. *Anesthesiology* **2000**, *93*, 1261–1270.

(12) Jouan-Hureau, V.; Audonnet-Blaise, S.; Lacatusu, D.; Krafft, M. P.; Dewachter, P.; Cauchois, G.; Stoltz, J. F.; Longrois, D.; Menu, P. *Transfusion* **2006**, *46*, 1892–1898.

(13) Sakai, H.; Yuasa, M.; Onuma, H.; Takeoka, S.; Tsuchida, E. *Bioconjugate Chem.* **2000**, *11*, 56–64.

(14) Vandegriff, K. D.; McCarthy, M.; Rohlf, R. J.; Winslow, R. M. *Biophys. Chem.* **1997**, *69*, 23–30.

(15) Manjula, B. N.; Tsai, A.; Upadhyay, R.; Perumalsamy, K.; Smith, P. K.; Malavalli, A.; Vandegriff, K.; Winslow, R. M.; Intaglietta, M.; Prabhakaran, M.; Friedman, M. J.; Acharya, A. S. *Bioconjugate Chem.* **2003**, *14*, 464–472.

blood.^{16,17} We reported previously that HbV suspended in plasma-derived HSA or rHSA was almost Newtonian: no aggregation was detected microscopically.^{3,18} In Japan, rHSA will soon be approved for clinical use.¹⁹ However, various plasma substitutes such as hydroxyethyl starch (HES), dextran (DEX), and modified fluid gelatin (MFG) are used worldwide.^{20–22} The selection among these plasma substitutes should be determined not only by safety and efficacy but also by price, experience of clinicians, and customs of respective countries.

Water-soluble polymers generally interact with particles such as polystyrene beads, silica, liposomes, and red blood cells (RBCs) to induce aggregation or flocculation.^{23–28} For that reason, it is important to determine the compatibility of HbV with these plasma substitutes. With that background, we studied the rheological properties of HbV suspended in these plasma substitute solutions for the first time using a complex rheometer and a microchannel array. This study provides a unique opportunity to investigate the rheology of a highly concentrated liposomal suspension.

Materials and Methods

Preparation of HbV. The HbV used for this study was prepared by Oxygenix Co. Ltd. (Tokyo) under sterile conditions, as reported previously.^{29–31} The Hb was purified from outdated donated blood provided by the Japanese Red Cross Society (Tokyo, Japan). The encapsulated purified Hb (38 g/dL) contained 14.7 mM pyridoxal 5'-phosphate (PLP; Sigma) as an allosteric effector at a molar ratio of PLP/Hb = 2.5. The lipid bilayer comprised a mixture of 1,2-dipalmitoyl-*sn*-glycero-3-phosphatidylcholine, cholesterol, and 1,5-bis-*O*-hexadecyl-*N*-succinyl-L-glutamate in a molar ratio of 5/5/1 (Nippon Fine Chemical Co. Ltd., Osaka, Japan) and 1,2-distearoyl-*sn*-glycero-3-phosphatidylethanolamine-*N*-poly(ethylene glycol) (NOF Corp., Tokyo, Japan, 0.3 mol % of the total lipid). The particle diameter was 279 ± 95 nm. The HbVs were suspended in a physiologic saline solution at [Hb] = 10 g/dL ([lipids] = ca. 6 g/dL) and were deoxygenated for storage with N₂ bubbling in vials.³²

Plasma Substitutes. The plasma substitutes used in this study are listed in Table 1. Recombinant human serum albumin (rHSA, $M_w = 67$ kDa, 25 wt %) was a gift from Nipro Corp. (Osaka, Japan). Before use, it was diluted to 5 wt % using saline solution (Otsuka Pharmaceutical Co. Ltd., Osaka, Japan). DEX solution ($M_w = 40$ kDa, 10 wt % in a physiological saline solution) was purchased from Kobayashi Pharmaceutical Co. Ltd. (Osaka, Japan). An HES₇₀ solution (Saline-HES, $M_w = 68$ kDa, 6 wt % in a physiological saline solution) was purchased from Kyorin Pharmaceutical Co. Ltd. (Osaka, Japan). An HES₁₃₀ solution (Voluven, $M_w = 130$ kDa,

Table 1. Plasma-Substitute Solutions and Their Physicochemical Properties^a

plasma-substitute solutions	M_w (kDa)	M_n (kDa)	M_w/M_n	conc (g/dL) in saline	COP (Torr)	viscosity (mPa·s) at 25 °C	
						at 10 s^{-1}	at 1000 s^{-1}
DEX	40 ^b	25 ^b	1.6	10 ^b	44	4.5	4.5
MFG	30 ^b	23 ^b	1.3	4 ^b	44	2.2	2.3
HES ₆₇₀	670 ^b	194 ^c	3.5	6 ^b	27	4.5	4.4
HES ₂₀₀	240 ^b	70 ^b	3.4	6	29	2.5	2.5
HES ₁₃₀	130 ^b	50 ^b	2.6	6 ^b	35	2.3	2.3
HES ₇₀	68 ^b	17 ^b	4.0	6 ^b	34	2.0	2.0
rHSA	67 ^b	67 ^b	1.0	5	19	1.3	1.2

^a The viscosities at 10 and 1000 s⁻¹ are almost identical, indicating that these polymer solutions are Newtonian fluids. (See Supporting Information). DEX, dextran; HES, hydroxyethyl starch; MFG, modified fluid gelatin; rHSA, recombinant human serum albumin; COP, colloid osmotic pressure. ^b Data provided by the manufacturer. ^c Calculated from the concentration dependence of COP (unpublished data).

6 wt % in a physiological saline solution) and powdered HES₂₀₀ (HES200/0.5, $M_w = 200$ kDa) were gifts from Fresenius Kabi AG (Homburg v.d.H., Germany). The HES₂₀₀ was dissolved in a physiological saline solution at 6 wt %. An HES₆₇₀ solution (Hextend, $M_w = 670$ kDa, 6 wt % in a physiological Ringer lactate solution) was obtained from Hospira, Inc. (Lake Forest, IL). An MFG solution (Gelofusin, $M_w = 30$ kDa, 4 wt % in a physiological saline solution) was a gift from B. Braun Melsungen AG (Melsungen, Germany). The COP was measured using a colloid osmometer (model 4420; Wescor, Inc., Logan, UT; molecular weight cutoff = 10 000).

Preparation of HbV Suspended in Plasma Substitutes and Blood Samples. HbV suspended in a saline solution was ultracentrifuged (20 000g, 30 min) to produce HbV-particle sediment. After the removal of the upper saline solution, a plasma substitute solution was added, and the HbV was redispersed by stirring and vortexing; the final concentration was adjusted to [Hb] = 10 g/dL. Flocculation of HbV was apparent because HbV tended to phase separate and precipitate gradually when HbV was suspended either in HES₆₇₀, HES₂₀₀, HES₁₃₀, DEX, or MFG. However, the supernatant was transparent and not colored. Before rheological measurements, we measured the particle diameters using a light-scattering method (PCS submicron particle analyzer; Beckman Coulter Inc.) after diluting the flocculated HbV with a normal saline solution. The particle diameters (nm) of redispersed HbV (HbV-DEX, 270 ± 81 ; HbV-HES₆₇₀, 292 ± 101 ; and HbV-MFG, 278 ± 90) were almost identical to that of the original HbV suspension (279 ± 95 nm). These results indicate that no hemolysis occurred and that no morphological change in the individual HbV particles occurred. Immediately before measurement, the suspension was filtered (0.45 μm pore size, Dismic; Toyo Roshi Kaisha Ltd., Tokyo, Japan). For comparison, fresh human blood was withdrawn with heparinized syringes from three donors. Measurements were performed within 6 h after withdrawal.

Viscoelastic Measurement of HbV Suspended in Plasma Substitutes. Steady-shear viscosity and shear stress measurements, a strain-sweep measurement, and the step-shear rate procedure (relaxation test) were performed using a rheometer (Physica MCR 301; Anton Paar GmbH, Graz, Austria). The cone diameter was 50 mm; the gap angle between the cone and plate was 1°. A parallel plate (50 mm diameter) was also used to confirm the influence of the interface between the plates and the test materials. All measurements were performed at 25 °C. About 650 μL of the sample suspension was sandwiched between the cone and plate. The excess solution was wiped out. For the steady-shear viscosity measurement, the shear rate was decreased from 10³ to 10⁻⁴ s⁻¹. The shear rate was increased from 10⁻⁴ to 10³ s⁻¹ to confirm the presence of dynamic hysteresis. In this case, a preconditioning operation was performed for 60 s at 1 s⁻¹ and then standing still for 300 s. Some variance in the data was apparent at a lower shear rate, and the averaged viscosities and standard deviations are shown with the data ($n = 3$).

(16) Sakai, H.; Masada, Y.; Horinouchi, H.; Yamamoto, M.; Ikeda, E.; Takeoka, S.; Kobayashi, K.; Tsuchida, E. *Crit. Care Med.* **2004**, *32*, 539–545.

(17) Yamazaki, M.; Aeba, R.; Yozu, R.; Kobayashi, K. *Circulation* **2006**, *114*, 1220–1225.

(18) Sakai, H.; Tsai, A. G.; Kerger, H.; Park, S. I.; Takeoka, S.; Nishide, H.; Tsuchida, E.; Intaglietta, M. *J. Biomed. Mater. Res.* **1998**, *40*, 66–78.

(19) Kobayashi, K. *Biologicals* **2006**, *34*, 55–59.

(20) Webb, A. R.; Nash, G. B.; Dormandy, J. A.; Bennett, E. D. *Clin. Hemorheol.* **1990**, *10*, 287–296.

(21) Webb, A. R.; Barclay, S. A.; Bennett, E. D. *Intensive Care Med.* **1989**, *15*, 116–120.

(22) Traylor, R. J.; Pearl, R. G. *Anesth. Analg.* **1996**, *83*, 209–212.

(23) Meyuhas, D.; Nir, S.; Lichtenberg, D. *Biophys. J.* **1996**, *71*, 2602–2612.

(24) Sunamoto, J.; Iwamoto, K.; Kondo, H. *Biochem. Biophys. Res. Commun.* **1980**, *94*, 1367–1373.

(25) Otsubo, Y. *Langmuir* **1990**, *6*, 114–118.

(26) Tilcock, C. P.; Fisher, D. *Biochim. Biophys. Acta* **1982**, *688*, 645–652.

(27) Neu, B.; Meiselman, H. J. *Biophys. J.* **2002**, *83*, 2482–2490.

(28) Goto, Y.; Sakakura, S.; Hatta, M.; Sugiura, Y.; Kato, T. *Acta Anaesthesiol. Scand.* **1985**, *29*, 217–223.

(29) Takeoka, S.; Ohgushi, T.; Terase, K.; Ohmori, T.; Tsuchida, E. *Langmuir* **1996**, *12*, 1755–1759.

(30) Sou, K.; Naito, Y.; Endo, T.; Takeoka, S.; Tsuchida, E. *Biotechnol. Prog.* **2003**, *19*, 1547–1552.

(31) Sakai, H.; Masada, Y.; Takeoka, S.; Tsuchida, E. *J. Biochem. (Tokyo)* **2002**, *131*, 611–617.

(32) Sakai, H.; Tomiyama, K.; Sou, K.; Takeoka, S.; Tsuchida, E. *Bioconjugate Chem.* **2000**, *11*, 425–432.

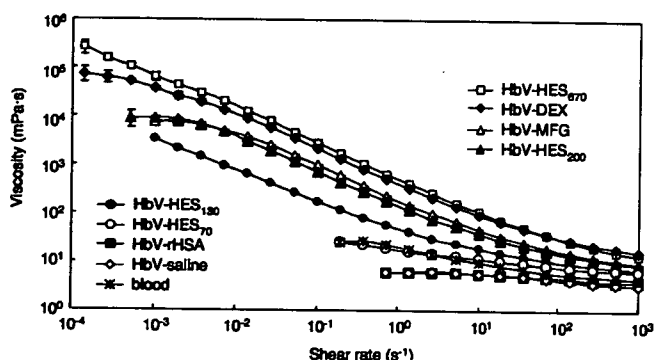


Figure 1. Viscosity of HbV suspended in various plasma-substitute solutions measured using an MCR 301 rheometer. The shear rate was decreased from 10^3 to 10^{-4} s^{-1} . Fluids with higher viscosity were measurable at a lower shear rate because of a sufficiently high strain of detection. Therefore, the low-viscosity HbV-rHSA and HbV-saline were measurable only above 0.7 s^{-1} . [Hb] = 10 g/dL, 25 °C. The blood data are inserted for comparison. Mean \pm SD ($n = 3$).

Strain-sweep measurements were carried out in the strain range of 0.01 – 100% at a frequency of 2 Hz using the same cone-and-plate geometry.

For the step-shear rate procedure, the viscosity of the HbV suspension was measured continuously for 120 s at a shear rate of 0.1 s^{-1} to confirm the constant viscosity. Next, the rotation speed of the cone plate was increased suddenly to attain a shear rate of 100 s^{-1} ; this condition was maintained for 220 s. Subsequently, the rotational speed was lowered suddenly to attain a shear rate of 0.1 s^{-1} ; this condition was maintained for 20 s. The response of the viscosity to the stepwise change of shear rates reflects the morphological change of HbV flocculation.

The respective dependencies of the storage modulus (G'), loss modulus (G''), and complex viscosity on the shear rate were analyzed using a dynamic capillary rheometer (DCR; Anton Paar GmbH) at shear rates of 5 – 330 s^{-1} at 37 °C.³³

Microchannel Flow Measurement. An array of microchannels (4.5 μm deep, 7 μm wide, 30 μm long, number 8736 in parallel, Bloody 6-7; Hitachi Haramachi Electronics Co. Ltd.) was used.³⁴ It was installed in a microchannel array flow analyzer (MC-FAN; Hitachi Haramachi Electronics Co. Ltd.). About 200 μL of the sample solution was inserted into the inlet syringe in order to flow through the microchannel array. The time necessary for a 100 μL suspension to pass through the channels at 20 cmH₂O, which corresponds to the capillary perfusion pressure, was measured ($n = 3$). Microscopic images were made of the flow patterns and the flocculate formation under a static condition (shutoff).

Results

Viscosity and Shear Stress of HbV Suspended in Plasma Substitutes. Figure 1 shows the viscosity of HbV suspended in various plasma substitute solutions when the shear rate decreased from 10^3 to 10^{-4} s^{-1} . The HbV suspended in rHSA was a nearly Newtonian fluid; no remarkable difference existed between HbV-rHSA and HbV suspended in saline. The respective viscosities of HbV-rHSA and HbV-HES₇₀ were nearly equal to those of human blood in comparison with other combinations. Because of the detection limit of shear strain of this rheometer and the very low viscosity of HbV-rHSA, only measurements above 5×10^{-1} s^{-1} were valid. However, HbV suspended in other polymer solutions—HES, DEX, and MFG—showed non-Newtonian properties with a high viscosity at lower shear rates, so-called

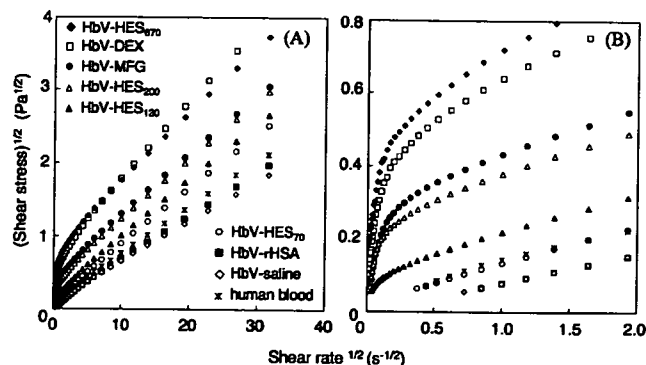


Figure 2. Casson plots of the square root of shear stress versus the square root of shear rate. These lines indicate that no clear stress yield exists. The graph is magnified in part B. Blood data are inserted for comparison.

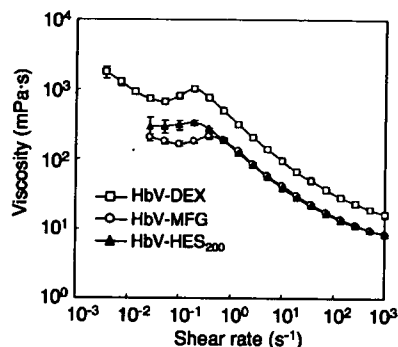


Figure 3. Shear thickening of HbV-DEX, HbV-HES₂₀₀, and HbV-MFG observed when the shear rate was increased in the opposite direction, from 10^{-4} to 10^3 s^{-1} . [Hb] = 10 g/dL, 25 °C. Mean \pm SD ($n = 3$).

shear-thinning, attributable to the flocculate formation of HbV. The viscosities were measurable over a wider range of shear rates.

The series of different molecular weights of HES for HbV-HES reflected the molecular weight dependence of the viscosity: higher-molecular-weight HES displayed enhanced HbV flocculation.

As a comparative study, the shear rate dependencies of the viscosities of all of the plasma substitute solutions were measured. All solutions showed constant viscosities, indicating that they are all Newtonian fluids,^{35–37} as shown in Table 1 and in Supporting Information.

Figure 2A,B shows Casson plots of shear stress versus the shear rate for all suspensions. HbV suspended in saline, rHSA, and HES₇₀ showed a relatively linear relationship. Other suspensions with high viscosities showed convex curves with marked deviations from the linear relationship, especially at lower shear rates. No stress yield is apparent for any line, even when the graph is magnified (Figure 2B).

Suspensions of HbV-DEX, HbV-HES₂₀₀, and HbV-MFG showed hysteresis of viscosity at lower shear rates (Figure 3) when the shear rate was changed in the opposite direction, from 10^{-4} to 10^3 s^{-1} . In addition, a shoulder or a peak was visible at

(35) Tiratmadja, V.; Dunstan, D. E.; Boger, D. V. *J. Non-Newtonian Fluid Mech.* **2001**, *97*, 295–301.

(36) Corry, W. D.; Jackson, L. J.; Seaman, G. V. *Biorheology* **1983**, *20*, 705–717.

(37) Wulansari, R.; Mitchell, J. R.; Blanchard, J. M. V.; Paterson, J. L. *Food Hydrocolloids* **1998**, *12*, 245–249.

(38) Buscall, R.; Mills, P. D. A.; Goodwin, J. W.; Lawson, D. W. *J. Chem. Soc., Faraday Trans. 1* **1988**, *84*, 4249–4260.

(39) Chen, M.; Russel, W. B. *J. Colloid Interface Sci.* **1991**, *141*, 564–577.

(33) Thurston, G. B. *Biophys. J.* **1972**, *12*, 1205–1217.

(34) Kikuchi, Y.; Sato, K.; Mizuguchi, Y. *Microvasc. Res.* **1994**, *47*, 126–139.

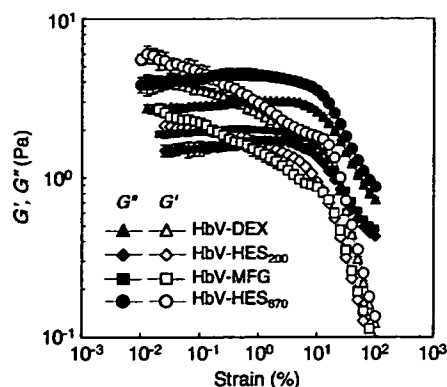


Figure 4. Strain dependence of the storage modulus (G') and loss modulus (G'') of HbV suspended in various plasma substitutes. [Hb] = 10 g/dL, $f = 2$ Hz. Mean \pm SD ($n = 3$).

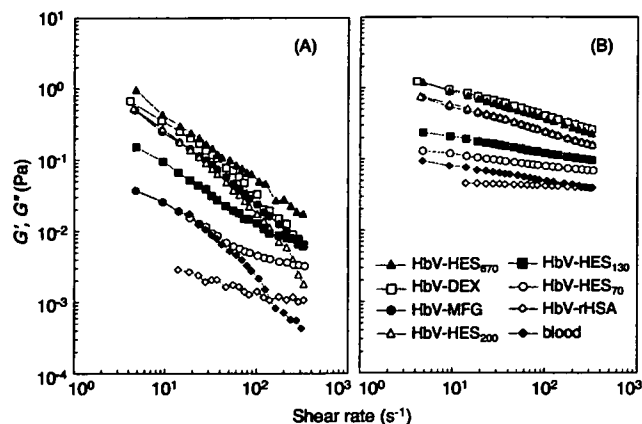


Figure 5. Respective shear rate dependencies of (A) the storage modulus, G' , and (B) the loss modulus, G'' , of HbV suspended in various plasma-substitute solutions as measured using a DCR rheometer. [Hb] = 10 g/dL, 37 °C. The blood curves are shown for comparison.

around 0.1 – 1 s^{-1} , indicating the presence of shear thickening in this range. However, suspensions with lower viscosities—HbV-HES₇₀ and HbV-HES₃₀—showed a monotonous shear-thinning viscosity change (data not shown). Measurements with the parallel plate at different thicknesses of the suspensions also showed the shear-thickening effect (data not shown), indicating that this phenomenon is reproducible and unrelated to a skidding effect at the interface of the plate and the suspension.

Measurement of the Storage Modulus (G') and Loss Modulus (G''). Figure 4 shows the strain dependence of the storage modulus (G') and loss modulus (G'') at [Hb] = 10 g/dL, $f = 2$ Hz. The elastic responses were predominant, producing higher G' values than G'' values at lower strains for the highly flocculated HbV suspensions: HbV-DEX, HbV-HES₆₇₀, HbV-HES₂₀₀, and HES-MFG. The G' value decreased gradually with increasing strain, but G'' was nearly constant at lower strains. Yielding points (critical strain γ_c) for these suspensions were at around 10% strain; in addition, the γ_c values for the three samples were almost identical, irrespective of the different levels of G'' . For HbV-rHSA, both G' and G'' were too small to detect and were therefore not included in the Figure.

Figure 5 shows the shear rate dependency of G' and G'' as measured using the capillary rheometer. At a lower shear rate, highly flocculated HbV suspensions HbV-DEX, HES₆₇₀-HbV, HbV-HES₂₀₀, and HbV-MFG showed high G' values. The contribution of G' decreased considerably when the HbV concentration was reduced at a constant polymer concentration.

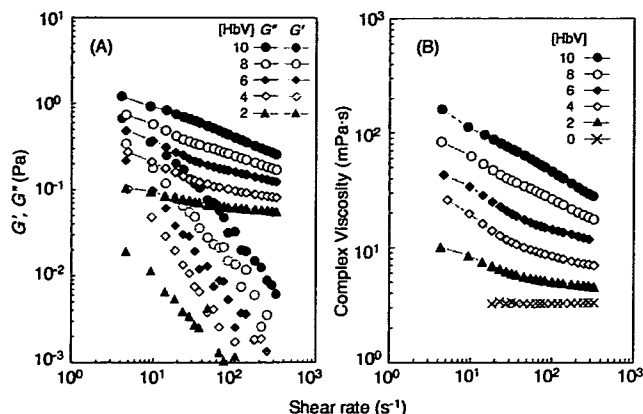


Figure 6. Representative profile of the concentration dependence (A) on G' and G'' and (B) on complex viscosity when the concentration of HbV in HbV-DEX was reduced from [Hb] = 10 to 0 g/dL at a constant DEX concentration (10 g/dL).

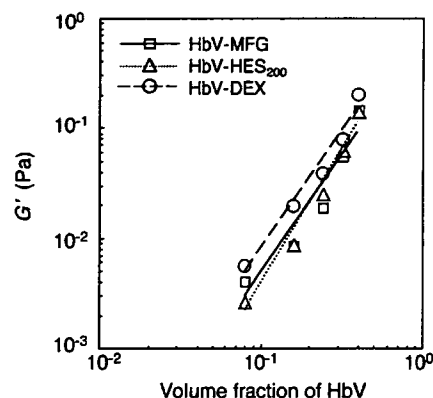


Figure 7. Logarithmic plots of G' at 18 s^{-1} vs ϕ (volume fraction of HbV) for HbV-DEX, HbV-HES₂₀₀, and HbV-MFG. For all cases, G' varies with ϕ following a power law of order 2.1–2.4. HbV-DEX, $G' \sim \phi^{2.13}$ ($R^2 = 0.9722$); HbV-HES, $G' \sim \phi^{2.45}$ ($R^2 = 0.9753$); and HbV-MFG, $G' \sim \phi^{2.14}$ ($R^2 = 0.9139$).

Figure 6A shows a representative profile of HbV-DEX at a constant dextran concentration. The complex viscosity of HbV-DEX depends strongly on the concentration of HbV (Figure 6B). For example, the complex viscosity at 320 s^{-1} decreased from 28 to 5 mPa·s when the Hb concentration decreased from 10 to 2 g/dL. Other plasma substitutes displayed similar profiles (data not shown).

The relationship between G' and ϕ (volume fraction of HbV) provides important information about the nature of particle flocculation.^{35,36} Figure 7 shows a logarithmic graph of G' at 18 s^{-1} versus ϕ for HbV-DEX, HbV-HES₂₀₀, and HbV-MFG. Those graphs show an almost linear relationship: G' varies with ϕ , following a power law of order 2.1–2.4.

Relaxation Test of HbV Suspended in Plasma Substitutes.

Figure 8A shows the response of viscosity to the rapid change of the shear rate. At a low shear rate (0.1 s^{-1}), the suspensions of HbV-DEX, HbV-HES₆₇₀, HbV-HES₂₀₀, and HbV-MFG showed very high viscosities because of flocculation. The viscosities decreased rapidly when the shear rate increased rapidly to 100 s^{-1} (which corresponds to the shear rate in a venule). The viscosities returned spontaneously to the original levels when the shear rate reverted rapidly to 0.1 s^{-1} . Figure 8B shows a magnification of the data for jumping points of Figure 8A, which clarifies that the suspension responded very promptly to the change in the shear rate. The reduction of viscosities that corresponded to the dissociation of flocculation was completed within 0.2 s,